HHS Public Access

Author manuscript

Cell Rep. Author manuscript; available in PMC 2019 February 12.

Published in final edited form as:

Cell Rep. 2018 November 20; 25(8): 2148–2162.e5. doi:10.1016/j.celrep.2018.10.074.

Activation of miR-21-Regulated Pathways in Immune Aging Selects against Signatures Characteristic of Memory T Cells

Chulwoo Kim[1,2], **Bin Hu**[1,2], **Rohit R. Jadhav**[1,2], **Jun Jin**[1,2], **Huimin Zhang**[1,2], **Mary M. Cavanagh**[1,2], **Rama S. Akondy**[3,4], **Rafi Ahmed**[3,4], **Cornelia M. Weyand**[1,2], and **Jörg J. Goronzy**[1,2,5,*]

[1]Division of Immunology and Rheumatology, Department of Medicine, Stanford University, Stanford, CA, USA

[2]Department of Medicine, Palo Alto Veterans Administration Healthcare System, Palo Alto, CA, USA

[3]Emory Vaccine Center, Emory University School of Medicine, Atlanta, GA, USA

[4]Department of Microbiology and Immunology, Emory University School of Medicine, Atlanta, GA, USA

[5]Lead Contact

SUMMARY

Induction of protective vaccine responses, governed by the successful generation of antigen-specific anti-bodies and long-lived memory T cells, is increasingly impaired with age. Regulation of the T cell proteome by a dynamic network of microRNAs is crucial to T cell responses. Here, we show that activation-induced upregulation of miR-21 biases the transcrip-tome of differentiating T cells away from memory T cells and toward inflammatory effector T cells. Such a transcriptome bias is also characteristic of T cell responses in older individuals who have increased miR-21 expression and is reversed by antagonizing miR-21. miR-21 targets negative feedback circuits in several signaling pathways. The concerted, sustained activity of these signaling path-ways in miR-21^{high} T cells disfavors the induction of transcription factor networks involved in memory cell differentiation. Our data suggest that curbing miR-21 upregulation or activity in older individuals may improve their ability to mount effective vaccine responses.

*Correspondence: jgoronzy@stanford.edu.

AUTHOR CONTRIBUTIONS

C.K., R.A., C.M.W., and J.J.G. designed and analyzed the experiments. C.K., B.H., J.J., H.Z., M.M.C., and R.S.A. performed the experiments. C.K. and R.R.J. analyzed the RNA-seq data. C.K. and J.J.G. wrote the manuscript, with all authors providing feedback.

DECLARATION OF INTERESTS

The authors declare no competing interests.

DATA AND SOFTWARE AVAILABILITY

The accession number for the RNA-seq data of miR-21^{high} and miR-21^{low} cells reported in this paper is SRA: SRP158689. The accession number for the RNA-seq data of effector cells from young and older individuals reported in this paper is SRA: SRP158502. Software DREVI is available at http://systemsbiology.columbia.edu/center-for-computational-biology-and-bioinformatics-c2b2.

SUPPLEMENTAL INFORMATION

Supplemental Information includes six figures and can be found with this article online at https://doi.org/10.1016/j.celrep.2018.10.074.

Graphical Abstract

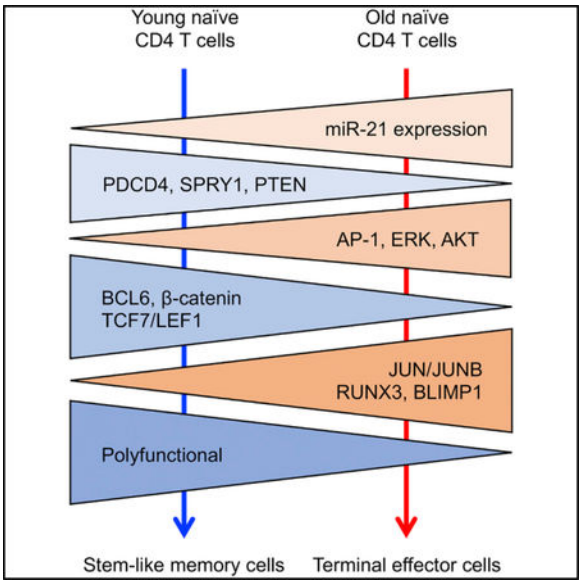

In Brief

A hallmark of the aging immune system is its failure to induce long-lived memory. Kim et al. report that increased expression of miR-21 in naive T cells from older individuals sustains signaling in the MAPK and AKT-mTORC pathways, disfavoring induction of transcription factor networks involved in memory cell generation.

INTRODUCTION

Vaccination is one of the most successful and safest interventions in modern medicine and has facilitated extinction of the smallpox virus and nearly complete eradication of some other devastating viruses, such as the poliomyelitis virus. Although vaccination programs have been extremely successful in children, they have been less beneficial in the older population. Infections, especially those of the respiratory tract by influenza or respiratory syncytial viruses as well as pneumococci or pertussis, and their complications are a frequent cause of morbidity and mortality in individuals older than 65 years (Beard et al., 2016). Because age demographics are rapidly changing worldwide, immune defects associated with increasing age have become a societal challenge, and the need for effective adult vaccination programs is now more urgent than ever.

The failure in older individuals to generate appropriate adaptive immune responses cannot be attributed to a single major defect (Goronzy and Weyand, 2017; Nikolich-Zugich, 2018). Contrary to earlier predictions, the size and diversity of the human $CD4^+$ T cell repertoire in older individuals is sufficient to respond to a diverse set of antigenic peptides (Qi et al., 2014). The $CD8^+$ T cell compartment is more affected by age, both in size and composition as well as in function and chromatin structure (Briceño et al., 2016; Czesnikiewicz-Guzik et al., 2008; Moskowitz et al., 2017; Nikolich-Zugich et al., 2012). Defects in T cell activation because of reduced dendritic cell function or T cell receptor (TCR) signaling have been

described (Li et al., 2012; Montgomery and Shaw, 2015) and may be overcome by adjuvanted vaccines or increasing the antigen dose (DiazGranados et al., 2014). The major T cell defect, however, appears to lie in cell differentiation and generation of T memory cells (Goronzy and Weyand, 2017). $CD4^+$ T cell responses of older individuals are biased toward the generation of inflammatory effector T cells that undergo attrition, and long-lived memory cells fail to develop (Fang et al., 2016; Qi et al., 2016).

T cell activation and differentiation into effector and memory T cells is regulated by a network of microRNAs shaping the T cell proteome (Dooley et al., 2013; Podshivalova and Salomon, 2013). Across differentiation states, the expression levels of individual microRNAs vary dramatically. Global microRNA deficiency, induced by deletion of microRNA-processing molecules, affects the proliferative expansion and effector function of T cells after activation. Elegant reconstitution experiments have identified microRNAs that account for these defects, such as miR-17 92, controlling proliferation, or miR-181a, setting the TCR activation threshold (Li et al., 2007). Specific microRNAs, including miR-17 ~92, have also been linked to polarization into effector lineages, frequently by directly targeting lineage-determining transcription factors (Baumjohann and Ansel, 2013). The miR-17 ~92 cluster is also important for the transition of $CD8^+$ T cells from effector to memory phenotypes. miR-17 ~92 is induced in $CD8^+$ T cells during the expansion phase following a viral infection but is downregulated during the contraction phase, enabling memory $CD8^+$ T cell formation, presumably by repressing activation of the AKT-mammalian target of rapamycin complex (mTORC) pathway (Wu et al., 2012). Although these studies were done in the mouse, the miR-17 ~92 cluster is conserved throughout mammalian species, suggesting that these findings are relevant for humans (Concepcion et al., 2012).

We and others have hypothesized that changes in microRNA expression with age account for the functional defects seen in Tcell responses in older individuals (Teteloshvili et al., 2015). Here we show that miR-21 is dynamically regulated after T cell activation. By controlling the sustained activation of the mitogen-activated protein kinase (MAPK) and AKT-mTORC signaling pathways, increased expression of miR-21 accounts for the preferential generation of inflammatory effector cells seen in T cell responses of older individuals while disfavoring the induction of transcriptional signatures characteristic of memory cells.

RESULTS

Regulation of miR-21 Expression after T Cell Activation Is Age-Dependent

miR-21 is dynamically regulated in T cell responses (Smigielska-Czepiel et al., 2013); upon activation with beads coated with anti-CD3 and anti-CD28 antibodies *in vitro*, miR-21 expression in naive $CD4^+$ T cells was robustly induced by more than 20-fold (Figure S1A). When assessing the influence of age, we found a 2-fold increase in miR-21 expression in naive $CD4^+$ T cells from older (65–85 years old) healthy adults compared with young (20–35 years old) individuals, with higher variance in the older population. This difference was maintained on day 3 following *in vitro* activation but was no longer seen on day 5, when miR-21 expression plateaued (Figure 1A).

miR-21 Induction Promotes Effector T Cell Differentiation

To examine whether the expression level of miR-21 influences T cell differentiation, we antagonized miR-21 by using a lentiviral transduction system. Naive $CD4^+$ T cells were activated with beads coated with anti-CD3 and anti-CD28 antibodies and transduced with a lentiviral vector expressing scrambled control RNA (ctrl) or anti-sense miR-21 (anti-miR-21) and a GFP reporter. Transduced cells were identified by GFP reporter activity. Transduction with the anti-miR-21 construct lowered the expression of miR-21 about 2-fold, approximately resembling the age-associated difference (Figure S1B). Partially counteracting the increase in miR-21 expression did not change $CD4^+$ T cell proliferation, as determined by Cell Trace Violet (CTV) dilution (Figure 1B), nor T cell apoptosis or recovery (Figures S1C and S1D).

We next utilized RNA sequencing (RNA-seq) to compare the gene expression profiles of control and anti-miR-21-transduced (miR-21^{low}) $CD4^+$ T cells activated for 5 days under non-polarizing conditions. miR-21^{low} cells had a distinct transcriptional signature, as shown by the shift in PC2 (accounting for 20% of the variance) in a principal-component analysis (PCA) (Figure 1C). No difference was seen in PC1 that reflected inter-individual differences. We identified 324 genes that were significantly upregulated and 304 genes that were downregulated in miR-21^{low} cells compared with control cells (adjusted $p < 0.1$). Cumulative distribution frequency plots showed that bioinformatically predicted miR-21 targets were upregulated with reduced miR-21 expression ($p < 0.0001$; Figure 1D).

Unopposed upregulation of miR-21 favored the induction of inflammatory and cytotoxic effector genes, including *IL2RA*, *GZMB*, *CCL3*, and *CCL4* (Figure 1E). These control-treated cells also had increased expression of inhibitory molecules, including *LAG3*, *DUSP5*, and *ENTPD1* (CD39), the latter recently described as a hallmark of short-lived effector T cells in humans (Fang et al., 2016). In contrast, reducing miR-21 expression during activation favored the transcription of genes related to memory T cell formation, such as *IL7R*, *BTLA*, *CD44*, and *CXCR3*, and genes in the WNT signaling pathway, which is associated with self-renewal, such as *CTNNB1* (β-catenin), *LEF1*, and *SOX4*. This bias was also reflected in transcription factor profiles; control cells expressed higher levels of transcription factors associated with effector differentiation, including *PRDM1* (BLIMP1), *JUNB*, *RUNX3*, *BHLHE40*, and *EGR1*, whereas miR-21^{low} cells had increased expression of *BCL6*, *TCF7*, and *LEF1*, involved in memory T cell differentiation (Kaech and Cui, 2012). None of these upregulated, memory cell-related genes was a predicted target of miR-21, implying that miR-21 affected pathways up-stream of their transcription. A global comparison using gene set enrichment analysis (GSEA) of the RNA-seq data supported this candidate gene-derived interpretation. Attenuating the increase in miR-21 expression favored the induction of a gene expression pattern that is characteristic of murine memory $CD8^+$ T cells (Kaech et al., 2002). In contrast, gene expression in activated $CD4^+$ T cells with unopposed miR-21 expression was more closely related to the transcriptome of terminal effector $CD8^+$ T cells (Sarkar et al., 2008; Figure 1F).

Functional Consequences of Increased miR-21 Expression

We next explored whether the effect of miR-21 expression on the transcriptome is functionally important and examined naive $CD4^+$ T cells from young and older individuals after transduction with anti-miR-21 and anti-CD3/CD28-mediated activation (Figure 2). Anti-miR-21-transduced $CD4^+$ T cells exhibited higher expression of the interleukin-7 (IL-7) receptor a chain (IL7Ra), a marker for memory precursor $CD8^+$ T cells (Kaech et al., 2003), compared with control cells on day 5. Flow cytometry also showed higher expression of CCR7 and CD62L in miR-21^{low} cells. Furthermore, reducing miR-21 expression resulted in lower expression of the effector cell markers IL2Rα and CD39 (Figure 2A). Phenotypic changes induced by antagonizing miR-21 were seen with $CD4^+$ T cells from young and older individuals.

Consistent with our transcriptome analysis, we observed higher BCL6 and TCF1 protein expression and reciprocal reduction of BLIMP1 in $CD4^+$ T cells with lowered miR-21 (Figures 2B and 2C). BCL6 and TCF1 are linked to memory and follicular helper (TFH) cell differentiation and antagonize *PRDM1* (BLIMP1) expression, a transcriptional repressor involved in cytotoxic $CD8^+$ T cell and Th1 cell differentiation (Crotty et al., 2010). Furthermore, we observed increased β-catenin expression in $CD4^+$ T cells with reduced miR-21 (Figure 2B). Along with TCF1 and LEF1, β-catenin is a transcriptional coactivator in canonical WNT signaling and a key regulator of the generation of stem cell-like memory T cells (Gattinoni et al., 2011).

To assess effector functions, $CD4^+$ T cells were re-stimulated on day 5 with phorbol 12-myristate 13-acetate (PMA) and ionomycin. miR-21^{low} cells had higher frequencies of IL-2- and tumor necrosis factor alpha (TNF-a)-producing cells but expressed less granzyme B than control cells. No difference in interferon γ (IFN-γ) production was observed (Figure 2D). This cytokine production profile of miR-21^{low} cells closely resembled that of memory precursor T cells (Sarkar et al., 2008).

Similar results after transduction with anti-miR-21 were obtained for $CD4^+$ T cells stimulated with the superantigen TSST-1 and dendritic cells (Figure S2) and anti-CD3/CD28-activated naive $CD8^+$ T cells (Figure S3).

Taken together, analysis of phenotypic markers, transcription factor networks, and effector functions supported the notion that induction of miR-21 expression upon T cell activation plays a regulatory role in effector differentiation, with high miR-21 upregulation promoting terminal effector cells and weaker upregulation favoring the development of memory precursor cells.

Increased miR-21 Expression with Older Age Favors Induction of a Terminal Effector Cell Expression Profile

The age-associated difference in miR-21 expression during early stages of naive $CD4^+$ T cell responses was of the same magnitude as seen with transduced anti-miR-21 (Figures 1A and S1B). The increased miR-21 expression in older individuals may therefore favor the generation of inflammatory effector T cells and select against transcriptome signatures pertinent for memory T cells. To test this hypothesis, we activated naive $CD4^+$ T cells from

young and older individuals with anti-CD3 and anti-CD28 beads for 5 days and performed transcriptome analysis by RNA-seq. We found that 794 genes were upregulated and 528 genes were downregulated in activated cells from older individuals compared with young adults (adjusted $p < 0.1$). Notably, differentially expressed genes between young and older individuals included many of the genes associated with effector and memory cell differentiation that were also influenced by miR-21 dysregulation. In line with the enhanced expression of inflammatory and cytotoxic effector genes and inhibitory molecules with strong upregulation of miR-21 expression (Figure 1E), activated cells from older individuals exhibited higher expression of *IL2RA*, *GZMB*, *CCL3*, *CCL4*, *LAG3*, *HAVCR2* (TIM3), and *DUSP5* and transcription factors such as *PRDM1* (BLIMP1), *JUNB*, and *RUNX3* than cells from young adults (Figure 3A). In contrast, the expression of memory-associated genes and transcription factors, including *SELL* (CD62L), *IL7R*, *CD28*, *TCF7*, *LEF1*, *ID3*, and *SOX4*, were lower in activated cells from older compared with those from young individuals (Figure 3A). Differential gene expression of key transcription factors was confirmed by RT-PCR in an independent cohort of young and older individuals. All expression differences, except for *BCL6*, remained statistically significant after controlling for multiple testing using Hochberg's stepdown adjustment (Figure 3B). The differences in *TCF7* and *PRDM1* expression were maintained until day 8 (Figure S4), suggesting that they did not reflect age-associated differences in activation kinetics.

Comparison of global gene expression profiles supported this interpretation. Applying GSEA, the differences in transcriptome signatures induced by lowering miR-21 upregulation in T cell responses correlated to those of young compared with older adults. Conversely, genes upregulated in older individuals were more likely enriched in control cells with unopposed miR-21 up-regulation (Figure 3C). Importantly, the expression level of miR-21 in naive T cells before activation was an excellent predictor of the gene expression pattern on day 5 after activation, inversely correlating with expression of memory transcription factors such as *TCF7* and *LEF1* and directly correlating with transcription factors that are highly expressed in effector T cells, such as *PRDM1* (BLIMP1), *JUNB*, and *RUNX3* (Figure 3D). The transcription factor *BCL6* did not correlate with miR-21 levels.

Because activated $CD4^+$ T cells from older individuals had a transcription factor signature resembling those of terminal effector cells induced under conditions of high miR-21 expression, we asked whether the effector molecule profiles differed accordingly with age. We activated naive $CD4^+$ T cells from young and older individuals and compared the frequencies of IL-2-, TNF-α-, and granzyme B-producing cells on day 5 after re-stimulation with PMA and ionomycin. Although TNF-a production was not different, activated $CD4^+$ T cells of older individuals produced more granzyme B and less IL-2 than cells from young adults, a pattern associated with short-lived terminal effector cells (Figure 3E). A preferential differentiation into inflammatory effector cells may explain the impaired vaccine responses that are seen with older age. To determine whether gene expression signatures of effector T cells after vaccination are inversely correlated with memory cell survival, we analyzed data (GEO: GSE86632) from a recent study with a live varicella zoster virus (VZV) vaccine (Qi et al., 2016). We compared the rate of decline of VZV-specific T cell frequencies from effector (days 8–14) with memory cells (day 28) with the gene expression profile of $CD4^+$ human leukocyte antigen DR ($HLA\text{-}DR^+$) $CD38^+$ activated T cells isolated

at the time of the $CD4^+$ T cell peak response. The decline in VZV-specific T cells during the contraction phase positively correlated with *GZMB* expression and negatively with *TCF7* expression (Figure 3F). These data are consistent with the model that preferential effector cell differentiation because of increased miR-21 levels in the early stages of the T cell response are associated with lower generation of longer-lived VZV-specific memory T cells.

miR-21 Targets PDCD4 to Increase AP-1 Activity

We explored whether signaling pathways regulated by miR-21 in the first days after activation influence whether T cells differentiate into proinflammatory effector cells or into memory T cells. Programmed cell death 4 (PDCD4) is one of the validated targets of miR-21 (Asangani et al., 2008) and has been shown to inhibit AP-1 activity (Yang et al., 2006). We confirmed that PDCD4 was a miR-21 target in T cells by transfecting naive $CD4^+$ T cells with miR-21-blocking locked nucleic acid (LNA21) or scrambled control and immunoblotting after 48-hr incubation without activation (Figure 4A). Upon T cell activation, *PDCD4* transcripts declined to bottoming between day 3 and day 4 and slightly rebounding on day 5 (Figure S5). miR-21^{low} cells expressing higher PDCD4 had reduced c-Jun N-terminal kinase (JNK) phosphorylation on day 3 after activation (Figure 4B). JNK is a kinase upstream of c-Jun and AP-1 activation. To directly monitor AP-1 activity, we transduced naive $CD4^+$ T cells with anti-miR-21 or control RNA after activation and additionally transfected the activated cells with an AP-1 reporter construct. Consistent with reduced JNK phosphorylation, AP-1 reporter activity was reduced in cells lentivirally transduced with anti-miR-21 (Figure 4C). These results indicate that upregulation of miR-21 expression activates AP-1 signaling by targeting the negative regulator PDCD4 upon T cell activation.

In line with increased miR-21 levels, we found that naive $CD4^+$ T cells of older individuals had lower expression of *PDCD4* throughout the activation and effector cell differentiation stages than naive $CD4^+$ T cells of young adults (Figure 4D). Activation of naive $CD4^+$ T cells induced a similar level of JNK phosphorylation in young and older individuals on day 3, suggesting that early signaling events are intact and not affected by age (Figures 4E and 4F). However, by day 4, JNK phosphorylation levels had substantially decreased in activated cells from young adults, whereas they were largely unchanged in activated cells from older individuals, suggesting that old but not young naive $CD4^+$ T cells have sustained AP-1 activity while differentiating (Figures 4E and 4F).

To determine the contribution of AP-1 signaling to effector T cell differentiation, naive $CD4^+$ T cells were activated with anti-CD3 and anti-CD28 beads in the presence of the AP-1 inhibitor SR11302. In these experiments, we predominantly analyzed $CD4^+$ T cells from older individuals (9 of 12 experiments for CD39, 12 of 12 for all other readouts). Pharmacologically inhibiting AP-1 activity enhanced IL7Rα and CCR7 expression and IL-2 and TNF-α production while reducing IL2Rα, CD39, and granzyme B expression on day 5 after activation, resembling the pattern in miR-21^{low} cells (Figure 4G). Similar results were obtained with c-FOS silencing (Figure 4H). Because AP-1 signaling induces miR-21 expression (Wang et al., 2014), treatment with the AP-1 inhibitor also dampened the upregulation of miR-21 after T cell activation, suggesting a positive feedback loop between

miR-21 expression, PDCD4 downregulation, and AP-1 activation (Figure 4I). Importantly, transfection of miR-21^{low} cells with PDCD4-targeting small interfering RNA (siRNA) partially reversed the effect of miR-21 silencing (Figure 4J).

miR-21 Activates the Mammalian Target of Rapamycin and Extracellular Signal-Regulated Kinase Signaling Pathways by Targeting PTEN and SPRY1

Signaling molecules directly targeted by miR-21 in naive CD4$^+$ T cells include PTEN and SPRY1, as shown by increased protein levels after antagonizing miR-21 (Figure 5A; Meng et al., 2007; Thum et al., 2008). Both *PTEN* and *SPRY1* decline upon T cell activation to slowly recover on day 5 (Figure S5). Increased SPRY1 is predicted to dampen extracellular signal-regulated kinase (ERK) phosphorylation (Thum et al., 2008). Increased PTEN should inhibit the AKT-mTORC pathway. Indeed, pharmacological inhibition of AKT reproduces the functional and phenotypic shifts seen with reducing miR-21 activity (Figure S6). On day 2 after activation, no major miR-21-dependent signaling differences were seen, as illustrated by the equal Ser^{235} and Ser^{236} phosphorylation of S6RP (Figure 5B) that occurs downstream of the mTORC1 as well as ERK signaling pathways (Roux et al., 2007). However, on day 3, antagonizing miR-21 showed the predicted effects on ERK, AKT, and mTORC1 phosphorylation (Figure 5C). The effect was most striking on S6 phosphorylation, with a large subpopulation of miR-21^{low} but not miR-21^{high} cells losing S6 phosphorylation between day 2 and day 3 (Figures 5B and 5C). To examine whether miR-21-mediated loss in PTEN and SPRY1 act additively or synergistically to maintain S6 phosphorylation, naive CD4$^+$ T cells were activated for 3 days and treated with combinations of the AKT inhibitor MK-2206 2HCl and the MEK1 and MEK2 inhibitor U0126 for 1.5 hr. S6 phosphorylation was lost in a subset of cells cultured with the AKT inhibitor as well as the MEK1 and MEK2 inhibitor at doses that only slightly blocked AKT or ERK phosphorylation (Figures 5D and 5E). Combining the MEK inhibitor with low concentration of the AKT inhibitor had an additive effect on S6 phosphorylation (Figure 5E).

Increased miR-21 Expression with Age Leads to Sustained Activation of the AKT-Mammalian Target of Rapamycin and ERK Signaling Pathways

Given the increase in miR-21 expression with age, we explored whether the similarities hold for the expression of PTEN and SPRY1. On days 3 and 4 after activation, naive CD4$^+$ T cells from older individuals expressed significantly lower levels of *PTEN* and *SPRY1* transcripts than cells from young adults (Figure 6A and 6B). This difference was attenuated on day 5, when expression of PTEN and SPRY1 started to rebound in spite of high miR-21 concentrations. The lower expression of these negative regulators appeared to be of functional importance to sustain S6 phosphorylation longer in activated T cells from older than young individuals (Figures 6C and 6D), reminiscent of the findings with cells differing in miR-21 expression (Figure 5). S6 phosphorylation was switched off in a subset of activated CD4$^+$ T cells between days 3 and 4 after activation, and this subset was larger in CD4$^+$ T cells from young individuals. Correspondingly, phosphorylation of upstream molecules decreased from day 3 to day 4 to a lesser extent in CD4$^+$ T cells from older adults, leading to a significant age-dependent difference in phosphorylated AKT, mammalian target of rapamycin (mTOR), and ERK on day 4 (Figures 6C and 6D). Again,

the differences seen for S6 phosphorylation were more pronounced than those in the upstream pathways, suggesting cooperative activity.

The relationship between upstream signaling pathways influenced by miR-21 and S6 phosphorylation was non-linear, with small upstream changes causing a digital response. To better describe the quantitative relationship between signaling molecules as influenced by age or miR-21 expression, we analyzed the flow data shown in Figures 6C and 6D using the conditional density resampled estimate of mutual information (DREMI) algorithm. Conditional density rescaled visualization (DREVI) plots showed a sharp transition from low to high S6 phosphorylation with an increase in ERK and AKT phosphorylation (Figure 6E). On day 3, the inflection points of ERK and AKT (i.e., the activation threshold of each signaling molecule at which transition of S6 phosphorylation occurs from low to high) were not different between young and older individuals. On day 4, young activated cells had a shift of the sigmoid curves toward higher ERK and AKT phosphorylation, indicating that higher activities were needed to induce S6 phosphorylation. In contrast, the activation thresholds of ERK and AKT signaling for S6 phosphorylation were maintained between day 3 and day 4 in $CD4^+$ T cells from old individuals (Figure 6E). These data show that small differences in ERK or AKT phosphorylation between young and old T cells was not sufficient to explain the large difference in digital responses, suggesting cooperative interactions of upstream pathways or activities of unidentified pathways. DREVI plots comparing miR-21^{low} and miR-21^{high} cells showed the same patterns, indicating that the mechanisms are related to miR-21 expression (Figure 6F).

DISCUSSION

Studies in murine models have achieved an excellent understanding of the transcription factor and microRNA (miRNA) networks that regulate T cell differentiation. Important roles have been identified for the opposing activities of the transcriptional repressors BCL6 and BLIMP1 (Crotty et al., 2010). miRNAs are critical for T cell differentiation and function, and the roles of selected miRNAs such as of those in the miR-17 ~92 cluster have begun to be deciphered (Baumjohann et al., 2013; Kang et al., 2013; Wu et al., 2012). Gene-regulatory pathways involved in the generation of TFH cells and memory precursor cells are at least in part overlapping and distinct from terminal effector T cells or TH1 cells (Choi et al., 2013; Crotty et al., 2010). These studies have generated the framework to understand and improve human vaccine responses in the aged host when the generation of protective adaptive immunity is impaired. Here we identify miR-21 as an important regulator to develop the transcriptional signature of an inflammatory effector cell versus that of a memory cell *in vitro*. Upon T cell activation, miR-21 was robustly induced, targeting negative regulators of three major signaling pathways: the ERK, AP-1, and AKT pathways. Small differences in miR-21 upregulation dramatically changed the expression and activity of transcriptional networks and, therefore, T cell differentiation, presumably through the cooperative activity of these pathways. Interventions to lower miR-21 expressions or to counteract miR-21's effects on signaling pathways resulted in $CD4^+$ T cells that expressed the homing receptors CCR7 and L-selectin, the cytokine receptor IL7Ra, and the transcription factor TCF1 and that were polyfunctional, all functional hallmarks of memory cells. *In vitro* studies cannot address the question of whether subdued miR-21 expression

also improves cell longevity, another requisite of memory cells compared with terminal effector T cells, and *in vivo* studies will be required to examine this point. The model that miR-21 controls an important decision point in the generation of long-lived memory cells is clinically relevant because miR-21 expression increases with age and could account for some of the findings characteristic of the T cell system in older individuals. The aging immune system is prone to inflammatory responses with the accumulation of functional effector T cells that have assumed features of innate effector cells (Pereira and Akbar, 2016; Warrington et al., 2001), and the T cell response is characterized by a preferential induction of effector T cells *in vitro* and a failure to generate memory T cells *in vivo* (Fang et al., 2016; Qi et al., 2016).

How does the ability of miR-21 to inhibit the development of a memory transcriptome concur with the current model of T cell differentiation? Obviously, AKT activation, subdued in miR-21^{low} cells, is a fundamental step in committing T cells to proliferation and differentiation. In our system, increased concentration of miR-21 within the first days after activation in older individuals was important to bias the transcriptome to effector instead of memory cells. However, although miR-21 effects on the expression of negative regulators were evident early after T cell activation, effects on signaling pathways were delayed, possibly because negative regulators are more efficacious when signaling intensities decline. Taken together, our data suggest that miR-21 upregulation functions mainly in sustaining signaling.

Our model is consistent with the observation that inhibition of mTORC1 signaling by rapamycin or by silencing RAPTOR during lymphocytic choriomeningitis virus (LCMV) infection favors differentiation of memory precursors and enhances memory cell number and function (Araki et al., 2009). Moreover, transgenic expression of constitutively active AKT in T cells inhibited the expression of WNT signaling molecules, resulting in failure to induce TCF1, important for memory T cell development (Kim et al., 2012). Also, IL-2 stimulation sustains activation of the phosphatidylinositol 3-kinase (PI3K)-AKT-mTOR pathway, promoting BLIMP1 expression and TH1 instead of TFH differentiation (Ray et al., 2015). In our data, we saw reduced CD25 expression on day 5 in miR-21^{low} cells as well as in young CD4^{+} T cells that preferentially develop a memory signature. Moreover, under conditions of reduced miR-21 expression, we see activated T cells lose S6 phosphorylation faster *in vitro*. *In vivo* after LCMV infection, p-S6^{low} CD8^{+} T cells were high in the expression of TCF1 (Delpoux et al., 2017). TCF1 is highly expressed in memory precursor CD8^{+} T cells (Zhou et al., 2010). In summary, reduced miR-21 upregulation reproduces several features that have been described to favor the generation of memory cells and that are deficient in CD4^{+} T cell responses from older individuals.

In addition to the PI3K-AKT-mTORC pathway, miR-21 also targets MAPK signaling pathways; in fact, we propose that not a single target but the additive or synergistic activities of several signaling events influenced by miR-21 account for the effect on T cell differentiation. We observed that miR-21 reduces the expression of the negative regulators SPRY1 and PDCD4, resulting in increased ERK and AP-1 pathway activation. In mice, Spry1 knockout T cells have increased TCR signaling, leading to ERK and AP-1 activation and effector functions, such as IFN-g and granzyme B production (Collins et al., 2012). Of

particular interest for T cell differentiation is the ability of miR-21 to influence AP-1 activity. We observed reduced JNK phosphorylation and AP-1 activity in miR-21^{low} T cells or young naive CD4^{+} T cells that preferentially developed a T memory-like transcriptome. Sustained AP-1 activity is important because of its ability to induce BLIMP1 transcription, which can be counteracted by BCL6. BLIMP1 induces terminal effector T cell differentiation and inhibits the function of BCL6 to generate TFH cells (Crotty et al., 2010; Kaech and Cui, 2012). The major target of miR-21 enhancing JNK phosphorylation and AP1 activity is PDCD4. In addition, miR-21 may influence AP-1 activity through its ability to sustain AKT activity that phosphorylates BACH2, leading to rapid degradation (Roychoudhuri et al., 2016). Sustained AP-1 activation in BACH2-deficient CD8^{+} T cells promotes terminal effector cell differentiation after viral infection, leading to impaired long-lived memory development (Roychoudhuri et al., 2016).

Taken together, miR-21 targets several signaling pathways with the net result of increased effector cell and decreased memory T cell differentiation. Activation of these signaling pathways is more sustained in T cell responses of older individuals, suggesting that attenuation of miR-21 expression may be beneficial for improving adaptive immunity after vaccination with age. Several mechanisms have been identified in regulating miR-21 expression. STAT3 has been shown to induce miR-21 transcription after stimulation with IL-21 in CD4^{+} T cells or with IL-6 in myeloma cells (Lo¨ffler et al., 2007; van der Fits et al., 2011); however, STAT3 is also important in the differentiation of TFH and memory cells (Cui et al., 2011; Schmitt et al., 2014), and it is therefore doubtful that interference with this pathway will be beneficial even when downregulating miR-21. Alternatively, inhibiting the forward feedback loop upregulating miR-21 transcription by temporary interference with AP-1 activity may be advantageous to induce memory T cells. Also, because miR-21 has generated interest as an oncogenic microRNA (oncomiRNA), several strategies to therapeutically target miR-21 *in vivo* are under development (Li and Rana, 2014).

STAR★METHODS

KEY RESOURCES TABLE

REAGENT or RESOURCE	SOURCE	IDENTIFIER
Antibodies		
CD3 (CD3-2)	Mabtech	Cat# 3605-1-1000; RRID: AB_907218
CD28 (CD28.2)	BD Biosciences	Cat# 555725; RRID: AB_396068
CD4 (RPA-T4)	BD Biosciences	Cat# 555349; RRID: AB_398593
CD8 (RPA-T8)	BD Biosciences	Cat# 560662; RRID: AB_1727513
CD3 (HIT3a)	BioLegend	Cat# 300330; RRID: AB_10551436
CD45RA (HI100)	BD Biosciences	Cat# 555488; RRID: AB_395879
CD45RO (UCHL1)	BD Biosciences	Cat# 555493; RRID: AB_395884
CCR7 (G043H7)	BioLegend	Cat# 353212; RRID: AB_10916390
IL7Ra (eBioRDR5)	Thermo Fisher Scientific	Cat# 12-1278-41; RRID: AB_10853334
CD62L (DREG-56)	BioLegend	Cat# 304822; RRID: AB_830801
CD25 (M-A251)	BD Biosciences	Cat# 561399; RRID: AB_10643029
CD39 (A1)	BioLegend	Cat# 328218; RRID: AB_2562897
IL-2 (MQ1-17H12)	BD Biosciences	Cat# 560708; RRID: AB_1727543
TNFα (MAb11)	BioLegend	Cat# 502930; RRID: AB_2204079
Granzyme B (GB11)	BD Biosciences	Cat# 560213; RRID: AB_1645453
IFN-γ (4S.B3)	BD Biosciences	Cat# 554552; RRID: AB_395474
BCL6 (K112-91)	BD Biosciences	Cat# 561525; RRID: AB_10898007
TCF1/TCF7 (S33-966)	BD Biosciences	Cat# 564217; RRID: AB_2687845
β-catenin (15B8)	eBioscience	Cat# 50-2567-42; RRID: AB_11218086
p-JNK (T183/Y185; N9-66)	BD Biosciences	Cat# 562480; RRID: AB_11153134
p-S6 (S235/S236; N7-548)	BD Biosciences	Cat# 561457; RRID: AB_10643763
p-AKT (S473; M89-61)	BD Biosciences	Cat# 560343; RRID: AB_1645397
p-mTOR (S2448; O21-404)	BD Biosciences	Cat# 564242; RRID: AB_2738695
p-ERK (T202/Y204; 20A)	BD Biosciences	Cat# 612593; RRID: AB_399876
BLIMP-1 (6D3)	Santa Cruz Biotechnology	Cat# sc-47732; RRID: AB_628168
PDCD4 (600-401-965)	Rockland Immunochemicals	Cat# 600-401-965; RRID: AB_828370
PTEN (138G6)	Cell Signaling Technology	Cat# 9559; RRID: AB_823618
SPRY1 (D9V6P)	Cell Signaling Technology	Cat# 13013
β-actin (13E5)	Cell Signaling Technology	Cat# 4970; RRID: AB_2223172
Bacterial and Virus Strains		
miRZip-scrambled hairpin vector	Systems Biosciences	Cat# MZIP000-PA-1
miRZip-21 anti-miR-21	Systems Biosciences	Cat# MZIP21-PA-1
Biological Samples		
Leukapheresis	Stanford blood center	N/A
Peripheral blood	Healthy volunteers	N/A
Chemicals, Peptides, and Recombinant Proteins		
Lymphoprep	STEMCELL Technologies	Cat# 07851
Fixable Viability Dye	Thermo Fisher Scientific	Cat# 65-0866-14

REAGENT or RESOURCE	SOURCE	IDENTIFIER
Human GM-CSF	R&D Systems	Cat# 215-GM-010
Human IL-4	R&D Systems	Cat# 204-IL-010
Human TNF-α	Peprotech	Cat# 300-01A
Human IL-2	Peprotech	Cat# 200-02
Prostaglandin E2	Sigma	Cat# P0409
SR11302, AP1 inhibitor	Tocris Bioscience	Cat# 2476
MK-2206 2HCl, AKT inhibitor	Selleckchem	Cat# S1078
U0126, ERK inhibitor	Tocris Bioscience	Cat# 1144
Hexadimethrine bromide (polybrene)	Sigma	Cat# H9268
Toxic shock syndrome toxin 1 (TSST-1)	Toxin Technology	Cat# TT606
hsa-miR-21-5p miRCURY LNA miRNA Inhibitor	QIAGEN (Exiqon)	Cat# YI04100689
miRCURY LNA miRNA Inhibitor Control	QIAGEN (Exiqon)	Cat# YI00199006
Critical Commercial Assays		
RosetteSep Human CD4+ T Cell Enrichment Cocktail	STEMCELL Technologies	Cat# 15062
EasySep Human Naive CD8+ T Cell Enrichment Kit	STEMCELL Technologies	Cat# 19158
CD45RO MicroBeads, human	Miltenyi Biotec	Cat# 130-046-001
CD14 MicroBeads, human	Miltenyi Biotec	Cat# 130-050-201
Dynabeads Human T-Activator CD3/CD28	Thermo Fisher Scientific	Cat# 11131D
CellTrace Violet Cell Proliferation Kit	Thermo Fisher Scientific	Cat# C34557
Fixation/Permeabilization Solution Kit	BD Biosciences	Cat# 554714
BD Cytofix Fixation Buffer	BD Biosciences	Cat# 554655
BD Phosflow Perm Buffer III	BD Biosciences	Cat# 558050
Annexin V apoptosis detection kit	BD Biosciences	Cat# 559763
RNeasy Plus Micro Kit	QIAGEN	Cat# 74034
mirVana miRNA Isolation Kit	Thermo Fisher Scientific	Cat# AM1560
Ovation Human FFPE RNA-Seq Library Systems	NuGEN	Cat# 0340, 0341
P3 primary cell Nucleofector Kit	Lonza	Cat# V4XP-3024
Power SYBR Green PCR Master Mix	Thermo Fisher Scientific	Cat# 4367659
Maxima First Strand cDNA Synthesis	Thermo Fisher Scientific	Cat# EP0741
miRCURY LNA RT Kit	QIAGEN (Exiqon)	Cat# 339340
Dual-Luciferase Reporter Assay System	Promega	Cat# E1910
Deposited Data		
RNA-seq data of miR-21^{high} and miR-21^{low} cells	This study	SRA: SRP158689
RNA-seq data of activated naive CD4^{+} T cells from young and older individuals	This study	SRA: SRP158502
Microarray data of VZV-specific CD4^{+} T cells	Qi et al., 2016	GEO: GSE86632
Experimental Models: Cell Lines		

REAGENT or RESOURCE	SOURCE	IDENTIFIER
HEK293T	ATCC	Cat# CRL-11268; RRID:CVCL_1926
Oligonucleotides		
SMARTApool c-FOS siRNA	Dharmacon	Cat# M-003265-01-0005
SMARTApool PDCD4 siRNA	Dharmacon	Cat# M-004438-03-0005
siGENOME Non-Targeting siRNA Pool	Dharmacon	Cat# D-001206-13-05
hsa-miR-21-5p miRCURY LNA miRNA PCR Assay	QIAGEN (Exiqon)	Cat# YP00204230
SNORD48(hsa) miRCURY LNA miRNA PCR Assay	QIAGEN (Exiqon)	Cat# YP00203903
Recombinant DNA		
psPAX2	Addgene	Cat#12260
pMD2.G	Addgene	Cat#12259
AP-1 luciferase reporter plasmid	Addgene	Cat#40342
pRL-SV40 renilla luciferase reporter	Promega	Cat# E2231
Software and Algorithms		
FlowJo	TreeStar	RRID:SCR_008520
Prism	GraphPad Software	RRID:SCR_002798
Website for DREVI software	Krishnaswamy et al., 2014	http://systemsbiology.columbia.edu/center-for-computational-biology-a
Website for gene set enrichment analysis (GSEA) software	The Broad Institute	http://software.broadinstitute.org/gsea/index.jsp

CONTACT FOR REAGENT AND RESOURCE SHARING

Further information and requests for resources and reagents should be directed to and will be fulfilled by the Lead Contact, Jörg J.

Goronzy (jgoronzy@stanford.edu).

EXPERIMENTAL MODEL AND SUBJECT DETAILS

Primary human cell isolation—Peripheral blood samples were obtained from 27 female and 12 male healthy individuals who did not have a history of autoimmune disease, diabetes mellitus, renal disease, cardiovascular disease or cancer except skin cancer. Individuals with hypertension or hypercholesterinemia were included if controlled on treatment. 19 of these 39 individuals were older than 60 years. In addition, samples were obtained from 128 blood or platelet donors. These samples were deidentified except for whether donors were younger than 35 years or older than 60 years. The studies were approved by the Stanford University Institutional Review Board, and participants gave informed written consent.

Untouched $CD4^+$ T cells were purified from peripheral blood or leukapheresis samples of healthy volunteers with a human $CD4^+$ T Cell enrichment kit (STEMCELL Technologies), followed by density gradient centrifugation using Lymphoprep (STEMCELL Technologies). Naive $CD4^+$ T cells were further isolated by negative selection with anti-CD45RO magnetic beads (Miltenyi Biotec). Peripheral blood mononuclear cells (PBMCs) were isolated by

density gradient centrifugation. Naive $CD8^+$ T cell were isolated from PBMCs using a human naive $CD8^+$ T cell isolation kit (STEMCELL Technologies). $CD14^+$ monocytes were isolated from PBMCs using anti-CD14 magnetic beads (Miltenyi Biotec). Purity of isolated cells was 90% or higher.

Cell lines—HEK293T cells (ATCC) were grown in Dulbecco's modified eagle medium (DMEM) supplemented with 10% fetal bovine serum and 100 U/ml penicillin and streptomycin (Thermo Fisher Scientific).

METHOD DETAILS

Primary cell culture—Isolated T cells were activated with Dynabeads Human T-Activator CD3/CD28 (Thermo Fisher Scientific) in RPMI 1640 (Sigma) supplemented with 10% fetal bovine serum and 100 U/ml penicillin and streptomycin (Thermo Fisher Scientific). For AP-1 or AKT inhibition experiments, naive $CD4^+$ T cells were activated with anti-CD3/anti-CD28 beads along with the AP-1 inhibitor SR11302 (10 mM, Tocris Bioscience) or the AKT inhibitor MK-2206 2HCl (1 uM, Selleckchem), respectively. DMSO (Sigma) was used for control treatment. For AKT and MEK1/2 inhibition experiments, activated cells were cultured with combinations of the AKT inhibitor MK-2206 2HCl (40–1000 nM, Selleckchem), MEK1/2 inhibitor U0126 (400 nM, Tocris Bioscience) or vehicle (DMSO, Sigma) for 1.5 hours.

Lentivirus production and transduction—To antagonize miR-21, we used the miRZip-21 lentiviral vector expressing anti-sense miR-21 (Systems Biosciences). miRZip-scrambled hairpin vector was used as a control (System Biosciences). The vector additionally contained a GFP reporter. Lentivirus was produced by transfection of a lentiviral vector, along with psPAX2 (Plasmid #12260; Addgene) and pMD2.G (Plasmid #12259; Add gene) expression vectors into HEK293T cells by using FuGENE (Promega). Lentiviral particles were collected 48 and 72 hours after transfection, filtered through a 0.45-mm syringe filter (Millipore), concentrated using Peg-it solution (System Biosciences) and titered on HEK293T cells. For lentiviral transduction, naive $CD4^+$ or $CD8^+$ T cells labeled with CellTrace Violet (Thermo Fisher Scientific) were activated with anti-CD3/anti-CD28 beads and transduced with a lentiviral vector expressing scrambled control RNA or anti-sense miR-21 at a multiplicity of infection of 10 in the presence of 8 mg/ml polybrene (Sigma) and 10 U/ml human IL-2 (Peprotech). After 36 hours, activated cells were washed and cultured on plates coated with 1 mg/ml anti-CD3 (CD3–2) plus 2 mg/ml soluble anti-CD28 Ab (CD28.2) and 10 U/ml human IL-2 (Peprotech).

T cell activation with superantigen—Dendritic cells (DCs) were generated from $CD14^+$ monocytes by culture in complete RPMI 1640 (Sigma) with 800 U/ml granulocyte-macrophage colony–stimulating factor and 1000 U/ml IL-4 (R&D Systems) for 6 days, followed by maturation with 1100 U/ml TNF-α (Peprotech) and 1 mg/ml prostaglandin E2 (Sigma) for 24 hours. Naive $CD4^+$ T cells were activated with anti-CD3/anti-CD28 beads and transduced with a lentiviral vector expressing scrambled control RNA or anti-sense miR-21. After 4 hours, cells were washed extensively to remove beads and lentivirus and

cultured with DCs at a ratio of 50 to 1 plus 1 ng/ml toxic shock syndrome toxin 1 (TSST-1, Toxin Technology) for 5 days.

Flow cytometry—For cell surface stains, cells were incubated with fluorescently conjugated antibodies in PBS containing 1% FBS at 4°C for 30 minutes. For intracellular cytokine assays, cells were re-stimulated with 25 ng/ml phorbol 12-myristate 13-acetate (PMA, Sigma) and 500 ng/ml ionomycin (Sigma) in the presence of Brefeldin-A (GolgiPlug, BD Biosciences) for 4 hours at 37°C. Cells were then incubated with cell-surface antibodies, permeabilized with Cytofix/Cytoperm kit (BD Biosciences) and stained with fluorescently labeled antibodies specific to the indicated cytokines. For staining of transcription factors and phosphorylated signaling proteins, cells were fixed with Cytofix buffer (BD Biosciences) for 10 minutes at 37°C, followed by permeabilization with Perm buffer III (BD Biosciences) for 30 minutes on ice. Cells were then incubated with fluorescently labeled antibodies for 60 minutes at room temper-ature. Annexin V apoptosis detection kit (BD Biosciences) was used to detect apoptotic cells, according to the manufacturer's instructions. Dead cells were excluded from the analysis using LIVE/DEAD Fixable Aqua (eBioscience). The following fluorochrome-conjugated antibodies were used for flow cytometry: anti-CD4 (RPA-T4), anti-CD8 (RPA-T8), anti-CD3 (HIT3a), anti-CD45RA (HI100), anti-CD45RO (UCHL1), anti-CCR7 (G043H7), anti-IL7Ra (eBioRDR5), anti-CD62L (DREG-56), anti-CD25 (M-A251), anti-CD39 (A1), anti-IL-2 (MQ1–17H12), anti-TNFα (MAb11), anti-Granzyme B (GB11), anti-IFN-γ (4S.B3), anti-BCL6 (K112–91), anti-TCF1/TCF7 (S33–966), anti-β-catenin (15B8), anti-p-JNK (T183/Y185; N9–66), anti-p-S6 (S235/S236; N7–548), anti-p-AKT (S473; M89–61), anti-p-mTOR (S2448; O21–404), anti-p-ERK (T202/Y204; 20A). Cells were analyzed on an LSRII or LSR Fortessa (BD Biosciences). Flow cytometry data was analyzed using FlowJo (TreeStar). To determine the relationship between signaling molecules, we used conditional density rescaled visualization (DREVI) as previously described (Krishnaswamy et al., 2014). DREVI plots of the phospho-flow data were generated using software available at http://systemsbiology.columbia.edu/center-for-computational-biology-and-bioinformatics-c2b2.

RNA sequencing and data analysis—To compare miR-21^{low} cells and control cells, naive CD4$^+$ T cells from four healthy individuals were activated with anti-CD3/anti-CD28 beads and transduced with a lentiviral vector expressing scrambled control RNA or anti-sense miR-21. On day 5 after activation, cells were re-stimulated with PMA/ionomycin for 3 hours and lentivirally-transduced GFP$^+$ CD4$^+$ T cells were then sorted to > 97% purity on FACSAria (BD Biosciences). To compare effector cells of young and older individuals, naive CD4$^+$ T cells from three young (20–35 year-old) and three older (63–85 year-old) individuals were activated with anti-CD3/anti-CD28 beads for 5 days. Total RNA was prepared using the RNeasy Micro Kit (QIAGEN) and RNA quality and quantity were examined by a 2100 Bioanalyzer (Agilent Technologies). cDNA synthesis and library preparation were performed with Ovation Human FFPE RNA-Seq Library Systems (NuGEN). Libraries were pooled and sequenced on an Illumina 2500 HiSeq (miR-21 samples) or NextSeq 500 (young/old comparison). RNA-seq reads were aligned to hg19 with TopHat2 (miR-21 samples) or STAR (young/old comparison) using GENCODE v19 splice junctions. Differential expression was tested using DESeq2. Principal component

analysis (PCA) was performed on counts from 5000 genes with the highest variance across samples. Genes were considered to be differentially expressed if Benjamini-Hochberg adjusted p value was less than 0.1. Cumulative distribution frequency plot was used to compare global gene expression changes with antagonizing miR-21, displaying the $\log_2$(anti-miR-21/ctrl) against the cumulative frequency of all, miR-21 and miR-181a target genes, respectively. Bioinformatically-predicted miR-21 and miR-181a targets were downloaded from TargetScan (http://www.targetscan.org) and top 100 predicted targets based on the TargetScan Context ++ score were included in the analysis (Agarwal et al., 2015).

Gene set enrichment analysis—Gene set enrichment analysis (GSEA) software from the Broad Institute (http://software.broadinstitute.org/gsea/index.jsp) was used to determine the enrichment of gene sets in miR-21^{low} or control cells. For comparative GSEA analyses, we used gene signatures associated with murine memory CD8$^+$ T cells over effector CD8$^+$ T cells (Kaech et al., 2002) and KLRG1^{high} terminal effector CD8$^+$ T cells over KLRG1^{low} memory precursor T cells (Sarkar et al., 2008) under GEO: GSE1000001, GSE10239, respectively.

Varicella zoster virus (VZV) vaccination—Frequencies of VZV-specific T cells determined by IFN-γ ELISPOT at day 8, 14 and 28 and gene expression in activated CD4$^+$ T cells after vaccination with the live VZV vaccine Zostavax were previously published (Qi et al., 2016). The decline in VZV-specific T cells from effector (day 8–14) to memory (day 28) time points was compared to expression levels of *GZMB* and *TCF7* in isolated CD4$^+$ HLA-DR$^+$ CD38$^+$ activated T cells at day 14 (GEO: GSE86632).

Transfection—To silence miR-21, naive CD4$^+$ T cells were transfected with either locked nucleic acid (LNA) miR-21 inhibitor or scrambled inhibitor negative control (Exiqon) using the Amaxa Nucleofector system and P3 primary cell Nucleofector Kit (Lonza). After 48 hours, PDCD4, PTEN, SPRY1 and b-actin expression was assessed by western blot. To silence c-FOS or PDCD4 expression in activated cells, naive CD4$^+$ T cells activated for 36 hours were washed and transfected with either SMARTApool c-FOS siRNA, SMARTApool PDCD4 siRNA or negative control siRNA (Dharmacon) using the Amaxa Nucleofector system and P3 primary cell Nucleofector Kit (Lonza). Cells were resting for 12 hours and cultured on plates coated with 1 mg/ml anti-CD3 (CD3–2; Mabtech) plus 2 ¼g/ml soluble anti-CD28 (CD28.2; BD Biosciences) and 10 U/ml human IL-2 (Peprotech). After 3 days, cells were harvested and analyzed.

RNA isolation and quantitative RT-PCR—Total RNA was isolated using either the RNeasy Plus Micro kit (QIAGEN) or a mirVana miRNA Isolation Kit (Ambion) and converted to cDNA using Maxima First Strand cDNA Synthesis Kits (Thermo Fisher Scientific). Quantitative RT-PCR was performed on the ABI 7900HT system (Applied Biosystems) using Power SYBR® Green PCR Master Mix (Thermo Fisher Scientific), according to the manufacturer's instructions. Oligonucleotide primer sets used are as follows: *TCF7*: F- CTGGCTTCTACTCCCTGACCT, R-ACCAGAACCTAGCATCAAGGA; *LEF1*: F- AGAACACCCCGATGACGGA, R-

GGCATCATTATGTACCCGGAAT; *BCL6*: F-GTTG TGGACACTTGCCGGAA, R-CTCTTCACGAGGAGGCTTGAT; *PRDM1*: F-AACTTCTTGTGTGGTATTGTCGG, R-CAGTGCTCGGTT GCTTTAGAC; *JUN*: F-AACAGGTGGCACAGCTTAAAC, R-CAACTGCTGCGTTAGCATGAG; *JUNB*: F-ACGACTCATACACAGCTAC GG, R-GCTCGGTTTCAGGAGTTTGTAGT; *RUNX3*: F-GCGAGGGAAGAGTTTCACCC, R-TTGATGGCTCGGTGGTAGGT; *PDCD4*: F-TATGATGTGGAGGAGGTGGATGTGA, R-CCTTTCATCCAAAGGCAAAACTACA; *PTEN*: F-GGAAGTCTATGTGATCAAGAAATCG, R-CAGAAGTTGAACTGCTAGCCTCTGGA; *SPRY1*: F-GAGAGAGATTCAGCCTACTGCT, R-GCAGGTCTTTTCACCACCGAA; *ACTB*: F-ATGGCCACGGCTGCTTCCAGC, R-CATGGTGGTGCCGCCAGACAG. Expression levels were normalized to *ACTB* expression and displayed as $2^{-\Delta\Delta Ct}$.

miRNA quantification—Total RNA was isolated with a mirVana miRNA Isolation Kit (Ambion) and reverse- transcribed to cDNA using the miRCURY LNA Universal RT microRNA cDNA synthesis kit (Exiqon). Mature miR-21 expression levels were assessed by quantitative RT-PCR using the miRCURY LNA UniRT PCR primer for miR-21–5p (Exiqon) and Power SYBR® Green PCR Master Mix (Thermo Fisher Scientific). SNORD48 (Exiqon) was used as internal control to normalize miR-21 expression.

Western blotting—Cells were lysed in RIPA buffer containing PMSF and protease and phosphatase inhibitors (Santa Cruz Biotechnology) for 30 minutes on ice. Proteins were separated on denaturing 4%–15% SDS-PAGE (Bio-Rad), transferred onto PVDF membrane (Millipore) and probed with antibodies to BLIMP-1 (6D3; Santa Cruz Biotechnology), PDCD4 (600–401-965; Rockland Immunochemicals), PTEN (138G6; Cell Signaling Technology), SPRY1 (D9V6P; Cell Signaling Technology) and β-actin (13E5; Cell Signaling Technology). Membranes were developed using HRP-conjugated secondary antibodies and Pierce ECL western blotting substrate (Thermo Fisher Scientific).

Luciferase reporter assay—Naive $CD4^+$ T cells were activated with anti-CD3/anti-CD28 beads and transduced with a lentiviral vector as described above. After 36 hours, activated cells were cotransfected with the AP-1 luciferase reporter plasmid (Plasmid #40342; Addgene) along with pRL-SV40 renilla luciferase reporter (Promega) using the Amaxa Nucleofector system and P3 primary cell Nucleofector Kit (Lonza). After 4 hours, activated cells were cultured on plates coated with 1 μg/ml anti-CD3 (CD3–2; Mabtech) plus 2 mg/ml soluble anti-CD28 (CD28.2; BD Biosciences) and 10 U/ml human IL-2 (Peprotech). On day 3 after activation, cells were lysed and luciferase reporter activity was measured with the Dual-Luciferase Reporter Assay System (Promega).

QUANTIFICATION AND STATISTICAL ANALYSIS

Statistical analysis was performed using Prism (GraphPad). Unless stated otherwise, data are presented as mean and error bars indicate the standard error of the mean. Paired or unpaired two-tailed Student's t tests were used for comparing two groups. A two-tailed Pearson's correlation test was used for correlation analysis. One-way ANOVA with Tukey's post hoc test was used for multi-group comparisons. To correct for multiple testing, we used the Benjamini–Hochberg method with a family-wise-error rate at the 0.05 level. Significance of

differences in cumulative distribution frequencies was estimated by Kolmogorov–Smirnov test. $p < 0.05$ was considered statistically significant. Statistical details and significance can be found in the figure legends.

Supplementary Material

Refer to Web version on PubMed Central for supplementary material.

ACKNOWLEDGMENTS

We thank Corey Cain, Lusijah Sutherland, and the Palo Alto VA Flow Cytometry Core for assistance with flow cytometry and cell sorting. This work was supported by the NIH (R01 AR042527, R01 HL117913, R01 AI108906, and P01 HL129941 to C.M.W. and R01 AI108891, R01 AG045779, U19 AI057266, R01 AI129191, and I01 BX001669 to J.J.G.). The content is solely the responsibility of the authors and does not necessarily represent the official views of the NIH.

REFERENCES

Agarwal V, Bell GW, Nam JW, and Bartel DP (2015). Predicting effective microRNA target sites in mammalian mRNAs. eLife 4, e5005.

Araki K, Turner AP, Shaffer VO, Gangappa S, Keller SA, Bachmann MF, Larsen CP, and Ahmed R (2009). mTOR regulates memory CD8 T-cell differentiation. Nature 460, 108–112. [PubMed: 19543266]

Asangani IA, Rasheed SA, Nikolova DA, Leupold JH, Colburn NH, Post S, and Allgayer H (2008). MicroRNA-21 (miR-21) post-transcriptionally downregulates tumor suppressor Pdcd4 and stimulates invasion, intravasa-tion and metastasis in colorectal cancer. Oncogene 27, 2128–2136. [PubMed: 17968323]

Baumjohann D, and Ansel KM (2013). MicroRNA-mediated regulation of T helper cell differentiation and plasticity. Nat. Rev. Immunol 13, 666–678. [PubMed: 23907446]

Baumjohann D, Kageyama R, Clingan JM, Morar MM, Patel S, de Kouchkovsky D, Bannard O, Bluestone JA, Matloubian M, Ansel KM, and Jeker LT (2013). The microRNA cluster miR-17 92 promotes TFH cell differentiation and represses subset-inappropriate gene expression. Nat. Immunol 14, 840–848. [PubMed: 23812098]

Beard JR, Officer A, de Carvalho IA, Sadana R, Pot AM, Michel JP, Lloyd-Sherlock P, Epping-Jordan JE, Peeters GMEEG, Mahanani WR, et al. (2016). The World report on ageing and health: a policy framework for healthy ageing. Lancet 387, 2145–2154. [PubMed: 26520231]

Briceño O, Lissina A, Wanke K, Afonso G, von Braun A, Ragon K, Miquel T, Gostick E, Papagno L, Stiasny K, et al. (2016). Reduced naı¨ve CD8(+) T-cell priming efficacy in elderly adults. Aging Cell 15, 14–21. [PubMed: 26472076]

Choi YS, Yang JA, Yusuf I, Johnston RJ, Greenbaum J, Peters B, and Crotty S (2013). Bcl6 expressing follicular helper CD4 T cells are fate committed early and have the capacity to form memory. J. Immunol 190, 4014–4026. [PubMed: 23487426]

Collins S, Waickman A, Basson A, Kupfer A, Licht JD, Horton MR, and Powell JD (2012). Regulation of $CD4^+$ and $CD8^+$ effector responses by Sprouty-1. PLoS ONE 7, e49801. [PubMed: 23166773]

Concepcion CP, Bonetti C, and Ventura A (2012). The microRNA-17–92 family of microRNA clusters in development and disease. Cancer J 18, 262–267. [PubMed: 22647363]

Crotty S, Johnston RJ, and Schoenberger SP (2010). Effectors and memories: Bcl-6 and Blimp-1 in T and B lymphocyte differentiation. Nat. Immunol 11, 114–120. [PubMed: 20084069]

Cui W, Liu Y, Weinstein JS, Craft J, and Kaech SM (2011). An inter-leukin-21-interleukin-10-STAT3 pathway is critical for functional maturation of memory CD8+ T cells. Immunity 35, 792–805. [PubMed: 22118527]

Czesnikiewicz-Guzik M, Lee WW, Cui D, Hiruma Y, Lamar DL, Yang ZZ, Ouslander JG, Weyand CM, and Goronzy JJ (2008). T cell sub-set-specific susceptibility to aging. Clin. Immunol 127, 107–118. [PubMed: 18222733]

Delpoux A, Lai CY, Hedrick SM, and Doedens AL (2017). FOXO1 oppo-sition of CD8$^+$ T cell effector programming confers early memory properties and phenotypic diversity. Proc. Natl. Acad. Sci. USA 114, E8865–E8874. [PubMed: 28973925]

DiazGranados CA, Dunning AJ, Kimmel M, Kirby D, Treanor J, Collins A, Pollak R, Christoff J, Earl J, Landolfi V, et al. (2014). Efficacy of high-dose versus standard-dose influenza vaccine in older adults. N. Engl. J. Med 371, 635–645. [PubMed: 25119609]

Dooley J, Linterman MA, and Liston A (2013). MicroRNA regulation of T-cell development. Immunol. Rev 253, 53–64. [PubMed: 23550638]

Fang F, Yu M, Cavanagh MM, Hutter Saunders J, Qi Q, Ye Z, Le Saux S, Sultan W, Turgano E, Dekker CL, et al. (2016). Expression of CD39 on Activated T Cells Impairs their Survival in Older Individuals. Cell Rep 14, 1218–1231. [PubMed: 26832412]

Gattinoni L, Lugli E, Ji Y, Pos Z, Paulos CM, Quigley MF, Almeida JR, Gostick E, Yu Z, Carpenito C, et al. (2011). A human memory T cell subset with stem cell-like properties. Nat. Med 17, 1290–1297. [PubMed: 21926977]

Goronzy JJ, and Weyand CM (2017). Successful and maladaptive T cell aging. Immunity 46, 364–378. [PubMed: 28329703]

Kaech SM, and Cui W (2012). Transcriptional control of effector and memory CD8+ T cell differentiation. Nat. Rev. Immunol 12, 749–761. [PubMed: 23080391]

Kaech SM, Hemby S, Kersh E, and Ahmed R (2002). Molecular and func-tional profiling of memory CD8 T cell differentiation. Cell 111, 837–851. [PubMed: 12526810]

Kaech SM, Tan JT, Wherry EJ, Konieczny BT, Surh CD, and Ahmed R (2003). Selective expression of the interleukin 7 receptor identifies effector CD8 T cells that give rise to long-lived memory cells. Nat. Immunol 4, 1191–1198. [PubMed: 14625547]

Kang SG, Liu WH, Lu P, Jin HY, Lim HW, Shepherd J, Fremgen D, Verdin E, Oldstone MB, Qi H, et al. (2013). MicroRNAs of the miR-17 92 family are critical regulators of T(FH) differentiation. Nat. Immunol 14, 849–857. [PubMed: 23812097]

Kim EH, Sullivan JA, Plisch EH, Tejera MM, Jatzek A, Choi KY, and Suresh M (2012). Signal integration by Akt regulates CD8 T cell effector and memory differentiation. J. Immunol 188, 4305–4314. [PubMed: 22467649]

Krishnaswamy S, Spitzer MH, Mingueneau M, Bendall SC, Litvin O, Stone E, Pe'er D, and Nolan GP (2014). Systems biology. Conditional den-sity-based analysis of T cell signaling in single-cell data. Science 346, 1250689. [PubMed: 25342659]

Li Z, and Rana TM (2014). Therapeutic targeting of microRNAs: current sta-tus and future challenges. Nat. Rev. Drug Discov 13, 622–638. [PubMed: 25011539]

Li QJ, Chau J, Ebert PJ, Sylvester G, Min H, Liu G, Braich R, Mano-haran M, Soutschek J, Skare P, et al. (2007). miR-181a is an intrinsic modu-lator of T cell sensitivity and selection. Cell 129, 147–161. [PubMed: 17382377]

Li G, Yu M, Lee WW, Tsang M, Krishnan E, Weyand CM, and Goronzy JJ (2012). Decline in miR-181a expression with age impairs T cell receptor sensitivity by increasing DUSP6 activity. Nat. Med 18, 1518–1524. [PubMed: 23023500]

Lo¨ffler D, Brocke-Heidrich K, Pfeifer G, Stocsits C, Hackermuller J, Kretzschmar AK, Burger R, Gramatzki M, Blumert C, Bauer K, et al. (2007). Interleukin-6 dependent survival of multiple myeloma cells involves the Stat3-mediated induction of microRNA-21 through a highly conserved enhancer. Blood 110, 1330–1333. [PubMed: 17496199]

Meng F, Henson R, Wehbe-Janek H, Ghoshal K, Jacob ST, and Patel T (2007). MicroRNA-21 regulates expression of the PTEN tumor suppressor gene in human hepatocellular cancer. Gastroenterology 133, 647–658. [PubMed: 17681183]

Montgomery RR, and Shaw AC (2015). Paradoxical changes in innate im-munity in aging: recent progress and new directions. J. Leukoc. Biol 98, 937–943. [PubMed: 26188078]

Moskowitz DM, Zhang DW, Hu B, Le Saux S, Yanes RE, Ye Z, Buen-rostro JD, Weyand CM, Greenleaf WJ, and Goronzy JJ (2017). Epige-nomics of human CD8 T cell differentiation and aging. Sci. Immunol 2, eaag0192.

Nikolich-Zugich J (2018). The twilight of immunity: emerging concepts in ag-ing of the immune system. Nat. Immunol 19, 10–19. [PubMed: 29242543]

Nikolich-Zugich J, Li G, Uhrlaub JL, Renkema KR, and Smithey MJ (2012). Age-related changes in CD8 T cell homeostasis and immunity to infec-tion. Semin. Immunol 24, 356–364. [PubMed: 22554418]

Pereira BI, and Akbar AN (2016). Convergence of Innate and Adaptive Im-munity during Human Aging. Front. Immunol 7, 445. [PubMed: 27867379]

Podshivalova K, and Salomon DR (2013). MicroRNA regulation of T-lymphocyte immunity: modulation of molecular networks responsible for T-cell activation, differentiation, and development. Crit. Rev. Immunol 33, 435–476. [PubMed: 24099302]

Qi Q, Liu Y, Cheng Y, Glanville J, Zhang D, Lee JY, Olshen RA, Weyand CM, Boyd SD, and Goronzy JJ (2014). Diversity and clonal se-lection in the human T-cell repertoire. Proc. Natl. Acad. Sci. USA 111, 13139–13144. [PubMed: 25157137]

Qi Q, Cavanagh MM, Le Saux S, Wagar LE, Mackey S, Hu J, Maecker H, Swan GE, Davis MM, Dekker CL, et al. (2016). Defective T Memory Cell Differentiation after Varicella Zoster Vaccination in Older Individuals. PLoS Pathog 12, e1005892. [PubMed: 27764254]

Ray JP, Staron MM, Shyer JA, Ho PC, Marshall HD, Gray SM, Laidlaw BJ, Araki K, Ahmed R, Kaech SM, and Craft J (2015). The interleukin-2-mTORc1 kinase axis defines the signaling, differentiation, and metabolism of T helper 1 and follicular B helper T cells. Immunity 43, 690–702. [PubMed: 26410627]

Roux PP, Shahbazian D, Vu H, Holz MK, Cohen MS, Taunton J, Sonenberg N, and Blenis J (2007). RAS/ERK signaling promotes site-spe-cific ribosomal protein S6 phosphorylation via RSK and stimulates cap-depen-dent translation. J. Biol. Chem 282, 14056–14064. [PubMed: 17360704]

Roychoudhuri R, Clever D, Li P, Wakabayashi Y, Quinn KM, Klebanoff CA, Ji Y, Sukumar M, Eil RL, Yu Z, et al. (2016). BACH2 regulates CD8(+) T cell differentiation by controlling access of AP-1 factors to enhancers. Nat. Immunol 17, 851–860. [PubMed: 27158840]

Sarkar S, Kalia V, Haining WN, Konieczny BT, Subramaniam S, and Ahmed R (2008). Functional and genomic profiling of effector CD8 T cell sub-sets with distinct memory fates. J. Exp. Med 205, 625–640. [PubMed: 18316415]

Schmitt N, Liu Y, Bentebibel SE, Munagala I, Bourdery L, Venuprasad K, Banchereau J, and Ueno H (2014). The cytokine TGF-b co-opts signaling via STAT3-STAT4 to promote the differentiation of human TFH cells. Nat. Immunol 15, 856–865. [PubMed: 25064073]

Smigielska-Czepiel K, van den Berg A, Jellema P, Slezak-Prochazka I, Maat H, van den Bos H, van der Lei RJ, Kluiver J, Brouwer E, Boots AM, and Kroesen BJ (2013). Dual role of miR-21 in CD4+ T-cells: activa-tion-induced miR-21 supports survival of memory T-cells and regulates CCR7 expression in naive T-cells. PLoS ONE 8, e76217. [PubMed: 24098447]

Teteloshvili N, Kluiver J, van der Geest KS, van der Lei RJ, Jellema P, Pawelec G, Brouwer E, Kroesen BJ, Boots AM, and van den Berg A(2015). Age-associated differences in MiRNA signatures are restricted to CD45RO negative T cells and are associated with changes in the cellular composition, activation and cellular ageing. PLoS ONE 10, e0137556. [PubMed: 26360056]

Thum T, Gross C, Fiedler J, Fischer T, Kissler S, Bussen M, Galuppo P, Just S, Rottbauer W, Frantz S, et al. (2008). MicroRNA-21 contributes to myocardial disease by stimulating MAP kinase signalling in fibroblasts. Nature 456, 980–984. [PubMed: 19043405]

van der Fits L, van Kester MS, Qin Y, Out-Luiting JJ, Smit F, Zoutman WH, Willemze R, Tensen CP, and Vermeer MH (2011). MicroRNA-21 expression in CD4+ T cells is regulated by STAT3 and is pathologically involved in Se´zary syndrome. J. Invest. Dermatol 131, 762–768. [PubMed: 21085192]

Wang L, He L, Zhang R, Liu X, Ren Y, Liu Z, Zhang X, Cheng W, and Hua ZC (2014). Regulation of T lymphocyte activation by microRNA-21. Mol. Immunol 59, 163–171. [PubMed: 24631982]

Warrington KJ, Takemura S, Goronzy JJ, and Weyand CM (2001). CD4+,CD28- T cells in rheumatoid arthritis patients combine features of the innate and adaptive immune systems. Arthritis Rheum 44, 13–20. [PubMed: 11212151]

Wu T, Wieland A, Araki K, Davis CW, Ye L, Hale JS, and Ahmed R (2012). Temporal expression of microRNA cluster miR-17–92 regulates effector and memory CD8+ T-cell differentiation. Proc. Natl. Acad. Sci. USA 109, 9965–9970. [PubMed: 22665768]

Yang HS, Matthews CP, Clair T, Wang Q, Baker AR, Li CC, Tan TH, and Colburn NH (2006). Tumorigenesis suppressor Pdcd4 down-regulates mitogen-activated protein kinase kinase kinase kinase 1 expres-sion to suppress colon carcinoma cell invasion. Mol. Cell. Biol 26, 1297–1306. [PubMed: 16449643]

Zhou X, Yu S, Zhao DM, Harty JT, Badovinac VP, and Xue HH (2010). Differentiation and persistence of memory CD8(+) T cells depend on T cell factor 1. Immunity 33, 229–240. [PubMed: 20727791]

Highlights

- Upregulation of miR-21 upon T cell activation promotes effector cell differentiation
- Expression of miR-21 in naive CD4 T cells increases with age
- T cell responses in old individuals favor effector over memory cell differentiation
- miR-21 attenuation induces transcription factor networks supportive of memory cells

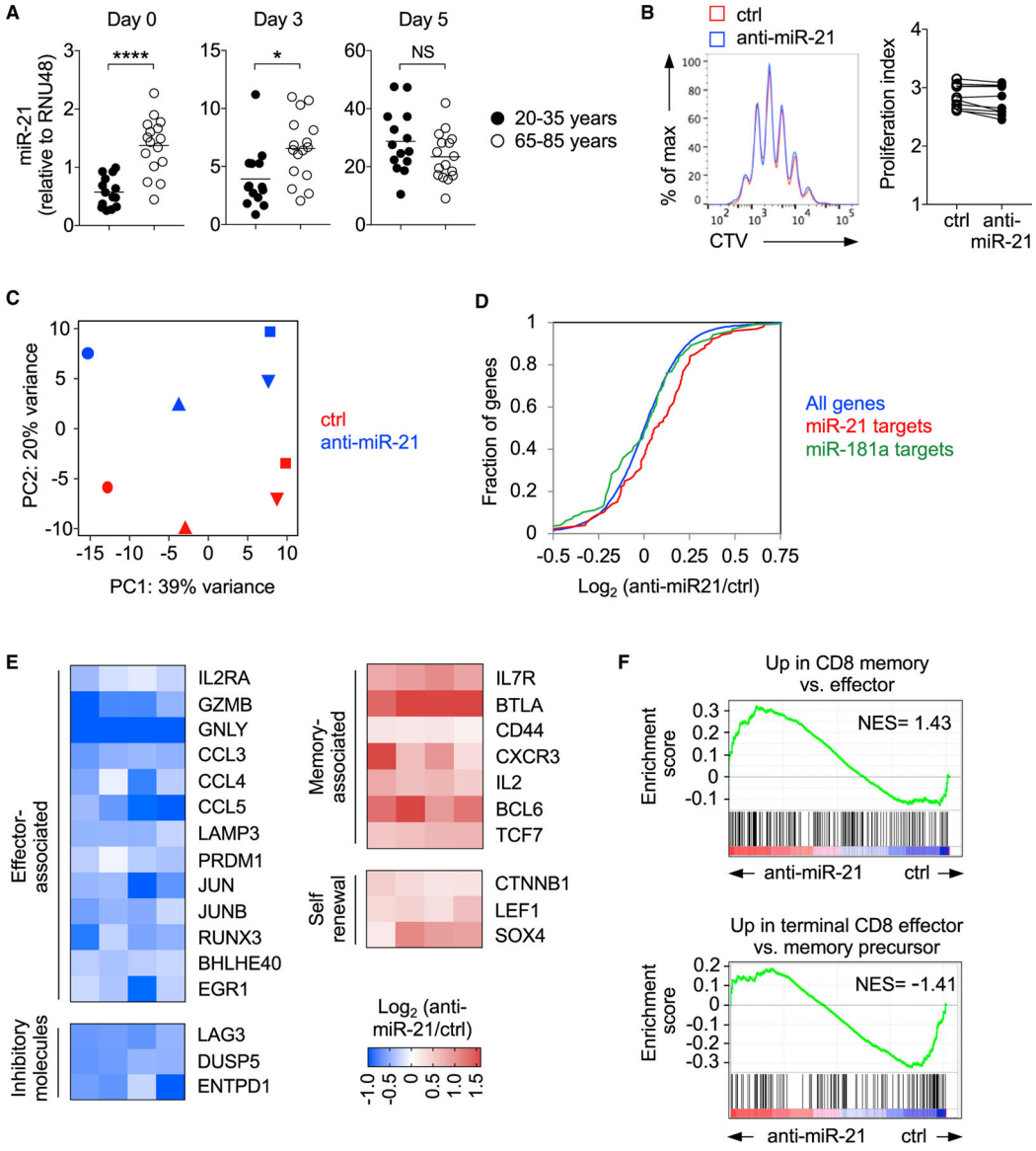

Figure 1. Age-Related Increase in miR-21 Expression Controls T Cell Differentiation

(A) Naive CD4$^+$ T cells were isolated from 14 20- to 35-year-old and 16 65- to 85-year-old healthy individuals and activated with anti-CD3 and anti-CD28 beads. miR-21 expression was measured at the indicated time points by qRT-PCR. Results are normalized to the expression of RNU48 and presented relative to those of unstimulated naive CD4$^+$ T cells. The horizontal lines represent mean values. *$p < 0.05$; ****$p < 0.0001$; NS, not significant; all by two-tailed unpaired t test.

(B) Naive CD4$^+$ T cells were activated with anti-CD3 and anti-CD28 beads and transduced with a lentiviral vector expressing scrambled control RNA or anti-sense miR-21 (anti-miR-21). The representative histogram shows proliferation of lentivirally transduced GFP$^+$ cells assessed by CellTrace Violet (CTV) dilution on day 5 (left). Proliferation indices are as determined by Flow-Jo (n = 10).

(C-F) Naive $CD4^+$ T cells were activated and transduced with a lentiviral vector as described in (B). GFP^+ cells transduced with control RNA or anti-miR-21 were sorted on day 5 after activation, followed by RNA-seq (n = 4).

(C) In a PCA, miR-21^{low} cells (blue) cluster separately from control-treated cells (red) in PC2. Each symbol represents paired replicates.

(D) Cumulative distribution plots show the mRNA fold change of miR-21^{low} cells relative to control cells for all genes (blue) and bioinformatically predicted miR-21 (red) or miR-181a (green) targets determined by TargetScan ($D = 0.3323$, $p < 0.0001$, by Kolmogorov-Smirnov test between all genes and miR-21 targets).

(E) Selected genes with significantly increased (red) and decreased (blue) expression in miR-21^{low} cells relative to those of control cells (adjusted $p < 0.1$) are shown as heatmaps of fold differences in paired samples.

(F) GSEA plots show the enrichment of gene signatures of murine $CD8^+$ memory (top left, $p = 0.002$, false discovery rate [FDR] = 0.062) and murine $KLRG1^+$ $CD8^+$ terminal effector (top right, $p = 0.021$, FDR = 0.206) compared with changes induced by antagonizing miR-21 expression.

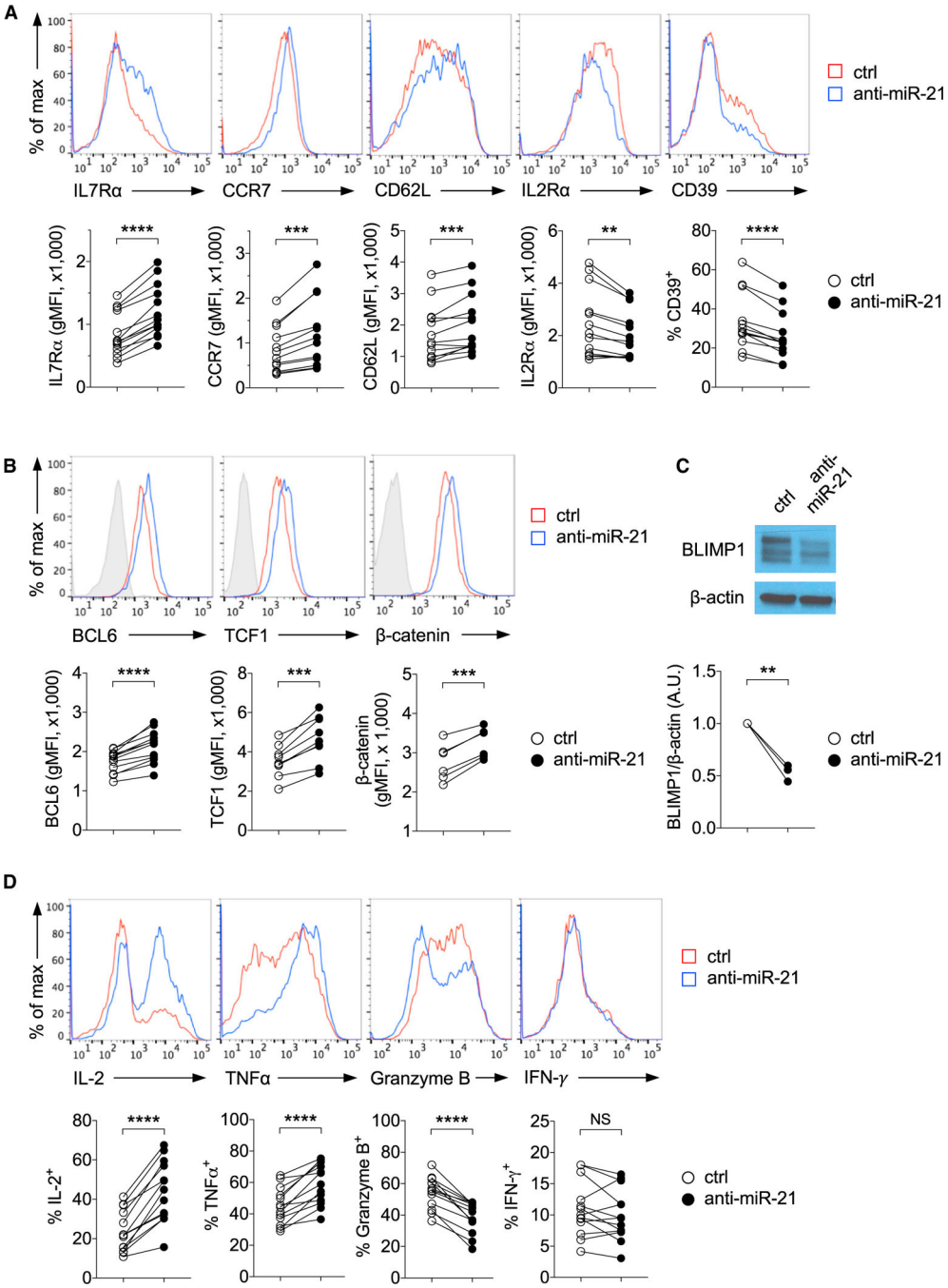

Figure 2. Functional Consequences of Increased miR-21 Expression

Naive CD4$^+$ T cells were activated with anti-CD3 and anti-CD28 beads and transduced with a lentiviral vector expressing either scrambled control RNA or anti-miR-21 for 5 days.

(A) Representative histograms of the surface expression of IL7Ra, CCR7, CD62L, IL2Ra, and CD39 in GFP$^+$ cells and results of paired samples from 13 (5–8 > 65 years) individuals are shown. Effect sizes were similar in young and old individuals.

(B) Representative histograms of intracellular expression of BCL6, TCF1, and b-catenin in GFP^+ cells and results from 6–12 (6–9 > 65 years) individuals. The filled gray histograms represent the fluorescence minus one (FMO) control.

(C) Representative western blot of BLIMP-1 expression in sorted GFP^+ cells and results from one old and two young individuals.

(D) Representative histograms and results from 10 to 13 experiments (5 from old individuals) of IL-2, TNF-a, granzyme B, and IFN-g production in GFP^+ cells after re-stimulation with PMA and ionomycin. $^{**}p < 0.01$, $^{***}p < 0.001$, $^{****}p < 0.0001$; all by two-tailed paired t test.

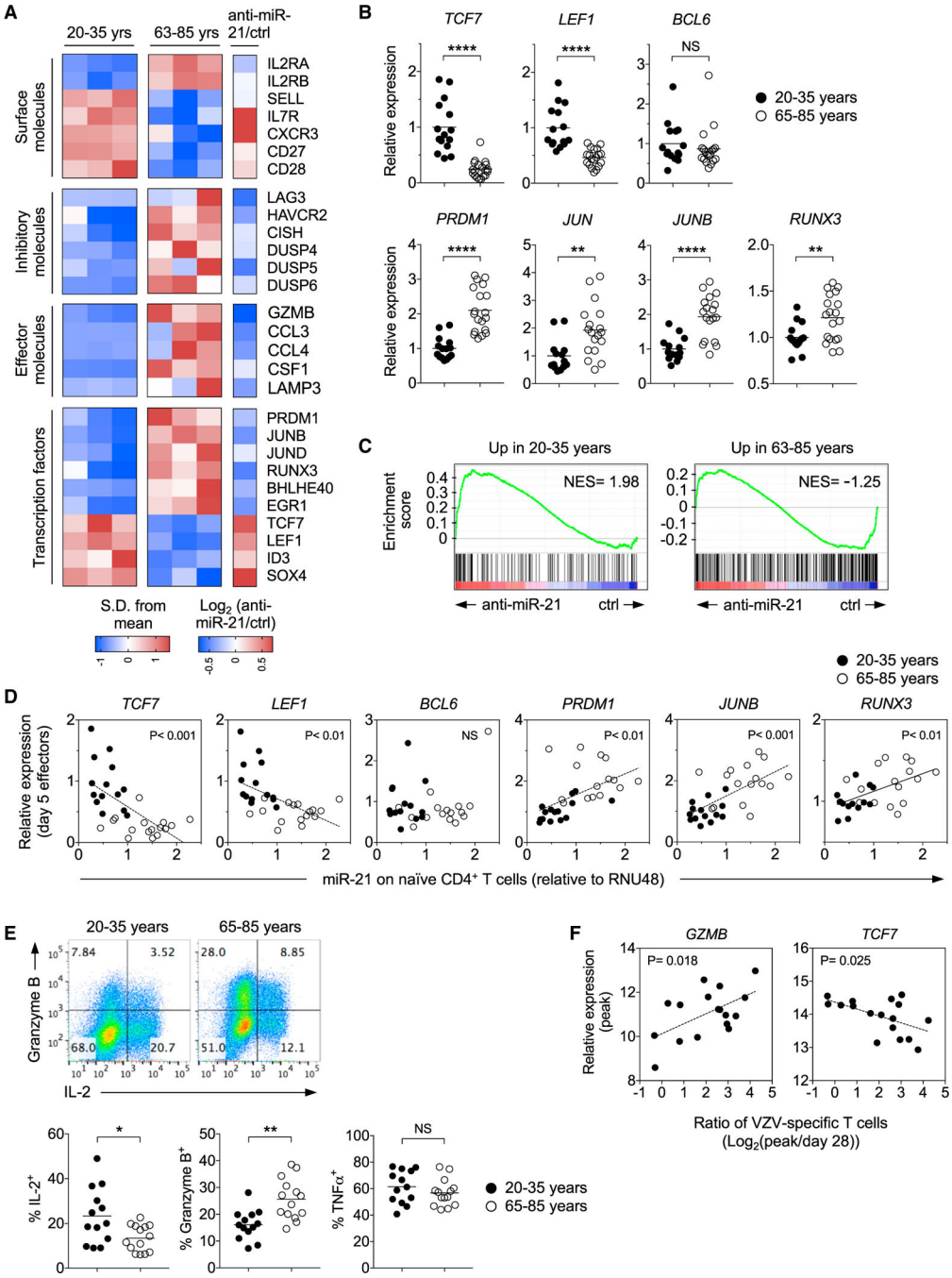

Figure 3. Activation of Naive CD4$^+$ T Cells from Older Individuals Preferentially Induces the Gene Signature of Effector Cells

(A) Naive CD4$^+$ T cells from three 20– 35-year-old and three 63- to 85-year-old individuals were activated with beads coated with anti-CD3 and anti-CD28 antibodies for 5 days, followed by RNA-seq. The heatmap indicates the relative expression of selected genes (adjusted $p < 0.1$).

(B) Differentially expressed genes from RNA-seq were confirmed by qRT-PCR in an independent cohort of 15 20- to 35-year-old and 19 65- to 85-year-old individuals on day 5 after activation. Results were normalized to *ACTB* and expressed relative to those of cells

from a young individual. The horizontal lines represent mean values (two-tailed unpaired t test).

(C) GSEA plots show the enrichment of a gene signature characteristic of young activated $CD4^+$ T cells in miR-21^{low} cells (left, $p < 0.001$, FDR = 0.001), whereas the gene signature of old activated $CD4^+$ T cells was related to that in $CD4^+$ T cells with unopposed miR-21 expression (right, $p = 0.028$, FDR = 0.265).

(D) The plots display miR-21 levels in unstimulated naive $CD4^+$ T cells for each individual presented in Figure 1A (young, closed circles; old, open circles) on the x axis and indicated transcript levels on day 5 after activation on the y axis (n = 30). Dotted lines indicate the best fit by linear regression. Pearson correlation coefficient and significance are shown.

(E) Naive $CD4^+$ T cells isolated from 20- to 35-year-old and 65- to 85-year-old healthy individuals were activated with beads coated with anti-CD3 and anti-CD28 antibodies for 5 days. Representative plots indicate intracellular production of IL-2 and granzyme B after re-stimulation with PMA and ionomycin. Numbers in quadrants indicate percent cells in each area. Graphs show the frequencies of IL-2-, granzyme B-, and TNF-a-producing cells from experiments with cells from 13 young and 14 older individuals. The horizontal lines represent mean values.

(F) After VZV vaccination, the VZV-specific T cell frequencies in peripheral blood mononuclear cells (PBMCs) were determined by IFN-g enzyme-linked immunospot (ELISPOT) at effector (days 8–14) and memory (day 28) time points. Plots display the ratio of the VZV-specific T cell frequencies on days 8–14 to day 28 for each individual on the x axis and *GZMB* or *TCF7* transcripts in isolated $CD4^+$ HLA-DR^+ $CD38^+$ activated T cells on day 14 on the y axis (n = 17). Dotted lines indicate the best fit by linear regression. Pearson correlation coefficient and significance are shown. *$p < 0.05$, **$p < 0.01$, ****$p < 0.0001$; all by two-tailed unpaired t test.

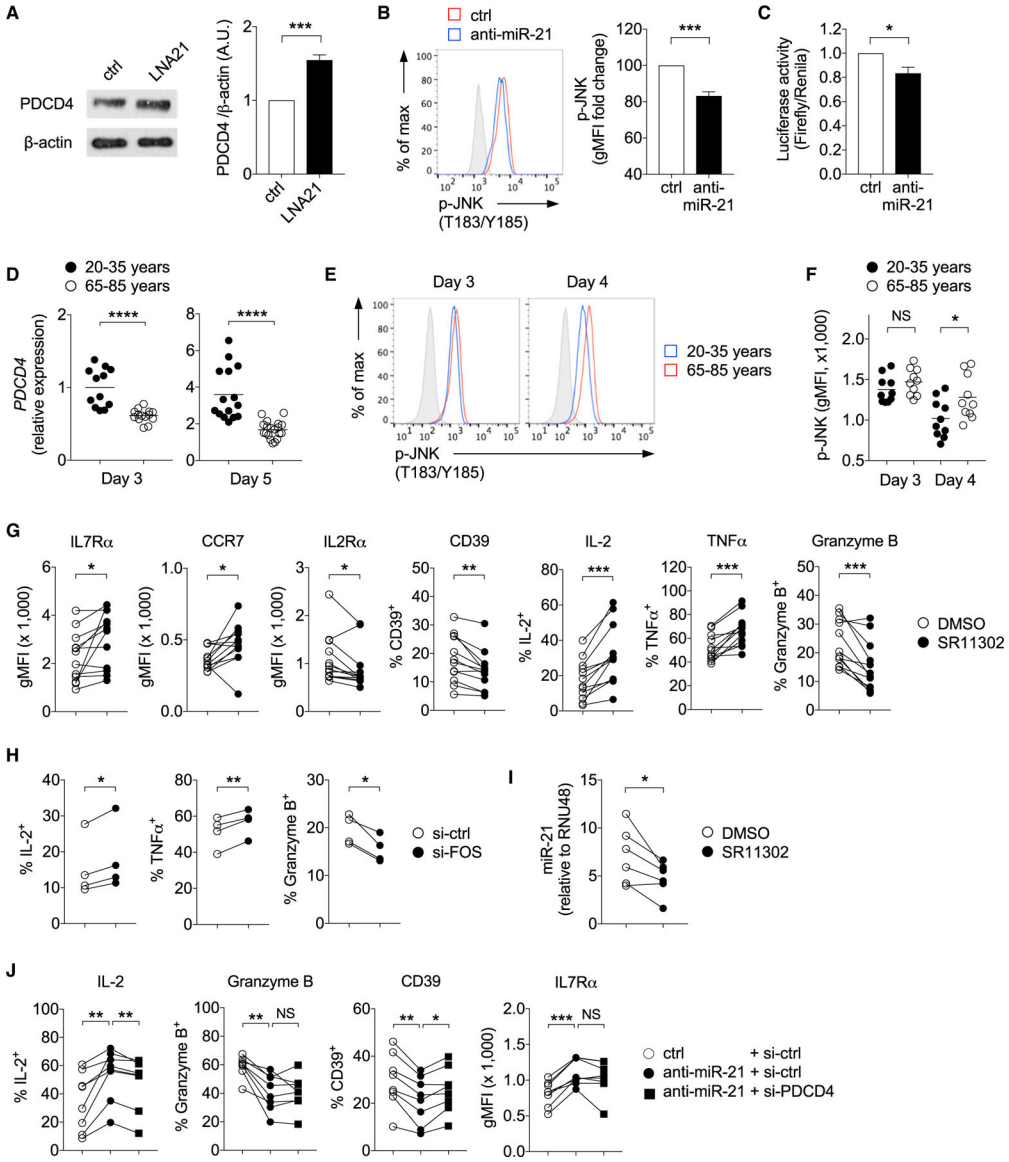

Figure 4. miR-21 Promotes Effector Cell Differentiation through AP-1 Activation

(A) Naive CD4$^+$ T cells were transfected with either scrambled control or miR-21-blocking locked nucleic acid (LNA21). After 48 hr, PDCD4 and b-actin expression were assessed by western blot. Representative blots and mean normalized intensities from four experiments are shown (mean ± SEM, two-tailed paired t test).

(B) Naive CD4$^+$ T cells were activated with anti-CD3 and anti-CD28 beads and transduced with a lentiviral vector expressing scrambled control or anti-miR-21. The representative histogram shows phosphorylated JNK in GFP$^+$ cells on day 3. The filled gray histogram represents unstimulated naive CD4$^+$ T cells. Results from 7 experiments are expressed relative to the geometric mean fluorescence intensity (MFI) of controls (mean ± SEM, two-tailed paired t test).

(C) Naive CD4$^+$ T cells were activated and transduced as described in (B) and co-transfected with the AP-1 luciferase reporter plasmid and the *Renilla* luciferase control construct. On

day 3, the activity of AP-1 firefly luciferase was measured and normalized to that of *Renilla* luciferase (n = 4, mean ± SEM, two-tailed paired t test).

(D–F) Naive $CD4^+$ T cells isolated from 20- to 35-year-old and 65- to 85-year-old individuals were activated with beads coated with anti-CD3 and anti-CD28 antibodies.

(D) *PDCD4* expression was quantified by RT-PCR on day 3 and day 5. Results are normalized to *ACTB* and presented relative to those of cells on day 3 from young individuals. The horizontal lines represent mean values (n = 12–19, two-tailed unpaired t test).

(E and F) Representative histograms (E) and geometric MFI of phosphorylated JNK on day 3 and day 4 from 10 individuals (F). The filled gray histograms represent unstimulated naive $CD4^+$ T cells. The horizontal lines represent mean values, and significance was calculated by two-tailed unpaired t test.

(G) Naive $CD4^+$ T cells from older adults were activated with anti-CD3 and anti-CD28 beads in the presence of either DMSO or the AP-1 inhibitor SR11302 for 5 days. Surface expression of IL7Ra, CCR7, IL2Ra, and CD39 and intracellular production of IL-2, TNF-a, and granzyme B after re-stimulation with PMA and ionomycin were assessed by flow cytometry (n = 12, two-tailed paired t test).

(H) Activated naive $CD4^+$ T cells were transfected with scramble control (si-ctrl) or c-FOS-specific siRNA (si-FOS) on day 2. IL-2, TNF-a, and granzyme B production were assessed on day 5 (n = 4, two-tailed paired t test).

(I) Naive $CD4^+$ T cells were activated as described in (G). miR-21 expression was measured on day 3 by qRT-PCR. Results are normalized to the expression of RNU48 and presented relative to those of unstimulated naive $CD4^+$ T cells (n = 6, two-tailed paired t test).

(J) Naive $CD4^+$ T cells were activated with anti-CD3 and anti-CD28 beads and transduced with a lentiviral vector expressing scrambled control RNA or anti-miR-21. After 36 hr, activated cells were transfected with si-ctrl or PDCD4-specific siRNA (si-PDCD4). The graphs show marker expression in GFP^+ cells on day 5 (n = 8, one-way ANOVA followed by Tukey's multiple comparison test).

*p < 0.05, **p < 0.01, ***p < 0.001, ****p < 0.0001.

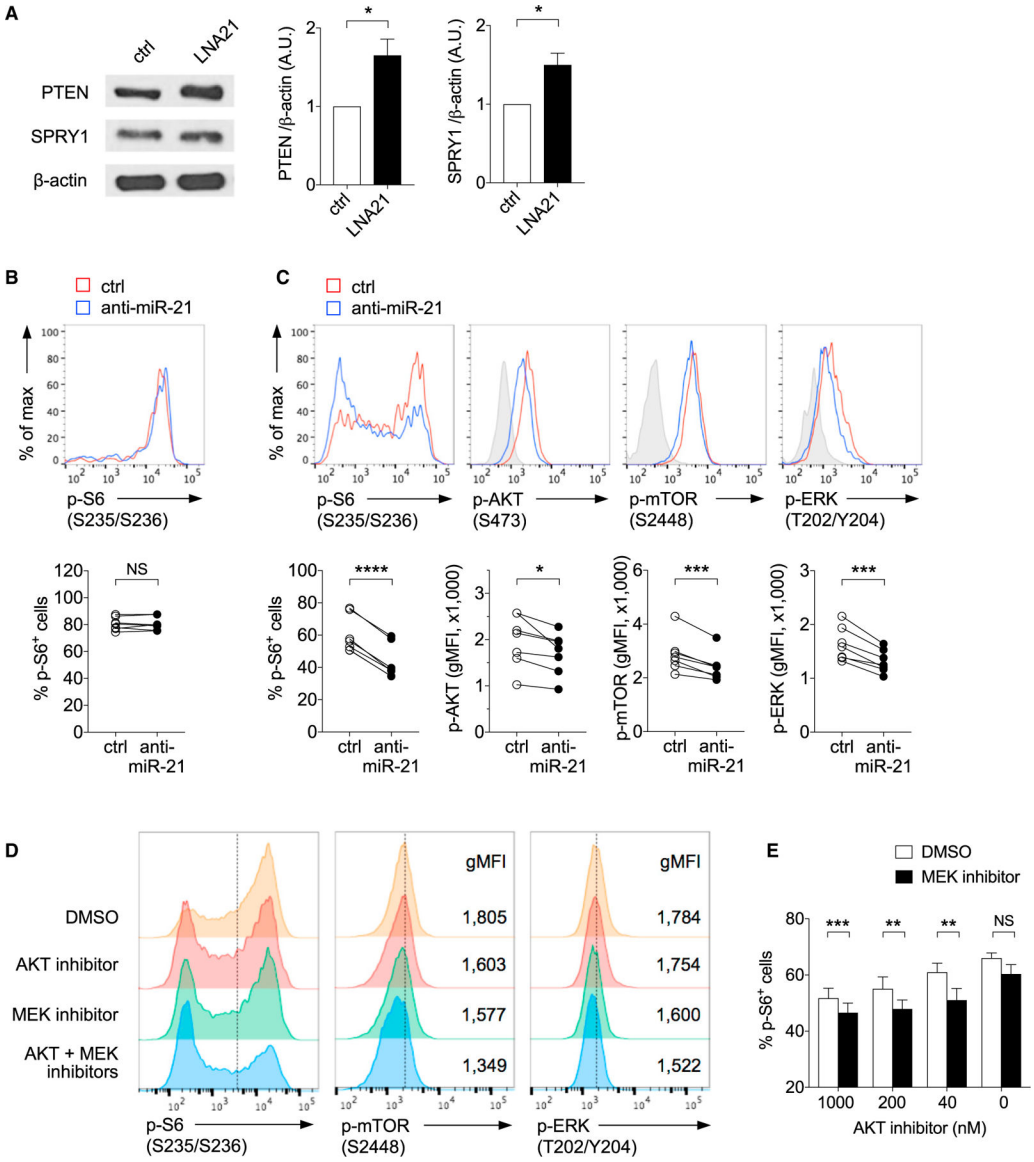

Figure 5. miR-21 Controls AKT and ERK Activation

(A) Naive CD4$^+$ T cells were transfected with either scrambled control or LNA21. Representative western blots and mean normalized band intensities of PTEN, SPRY1, and b-actin expression after 48 hr are shown (n = 3–4, mean ± SEM).

(B and C) Naive CD4$^+$ T cells from young and older individuals were activated with anti-CD3 and anti-CD28 beads and transduced with a lentiviral vector expressing scrambled control RNA or anti-miR-21.

(B) Representative histogram of phosphorylated S6 in GFP$^+$ cells on day 2 and results from 7 individuals.

(C) Representative histograms of phosphorylated S6, AKT, mTOR, and ERK in GFP$^+$ cells on day 3 and results of paired samples from 7 individuals. The filled gray histograms represent unstimulated naive CD4$^+$ T cells.

(D and E) Naive $CD4^+$ T cells from healthy adults were activated with anti-CD3 and anti-CD28 beads. On day 3, activated cells were treated with combinations of the AKT inhibitor MK-2206 2HCl and the MEK1 and MEK2 inhibitor U0126 for 1.5 hr.

(D) Representative histograms show phosphorylated S6, mTOR, and ERK in cells treated with combinations of 40 nM of the AKT inhibitor and 400 nM of MEK1 and MEK2 inhibitor. Numbers in histograms indicate geometric MFI of p-mTOR and p-ERK.

(E) Graphs depicting the frequencies of cells with phosphorylated S6 cultured with the indicated concentrations of the AKT inhibitor in the presence or absence of 400 nM of the MEK1 and MEK2 inhibitor (n = 4, mean ± SEM).

*p < 0.05, **p < 0.01, ***p < 0.001, ****p < 0.0001; all by two-tailed paired t test.

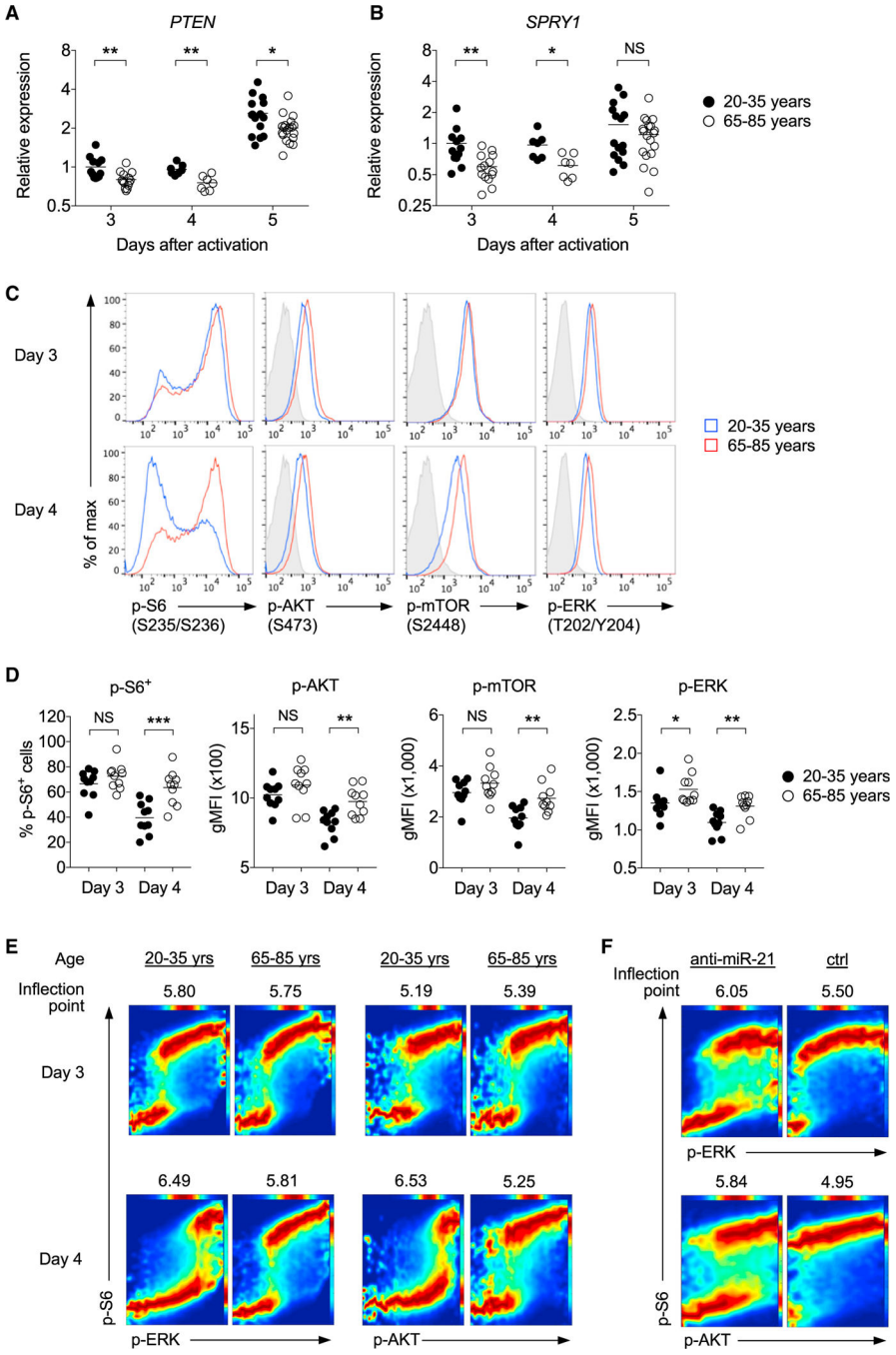

Figure 6. Sustained Activation of the AKT and ERK Signaling Pathways in Old Naive CD4$^+$ T Cells

(A and B) Naive CD4$^+$ T cells isolated from 20- to 35-year old and 65- to 85-year-old individuals were activated with beads coated with anti-CD3 and anti-CD28 antibodies. Expression of *PTEN* (A) and *SPRY1* (B) was measured by qRT-PCR on day 3, 4, and 5. Results are normalized to *ACTB* and presented relative to those of cells on day 3 from young individuals. The horizontal lines represent mean values (n = 8–19, two-tailed unpaired t test).

(C and D) Representative histograms (C) and phosphorylated S6, AKT, mTOR, and ERK on day 3 and day 4 from ten individuals (D) are shown. The filled gray histograms represent unstimulated naive $CD4^+$ T cells. The horizontal lines represent mean values (two-tailed unpaired t test).

(E) Representative conditional density rescaled visualization (DREVI) plots show DREMI analysis of the relationship between p-ERK (left) or p-AKT (right) with S6 phosphorylation in naive $CD4^+$ T cells from young and older individuals on days 3 and 4 after activation with anti-CD3 and anti-CD28 beads.

(F) DREMI analysis of miR-21^{high} and miR-21^{low} cells as described in (E).

*$p < 0.05$, **$p < 0.01$, ***$p < 0.001$.

REAGENT or RESOURCE	SOURCE	IDENTIFIER
Antibodies		
CD3 (CD3-2)	Mabtech	Cat# 3605-1-1000; RRID: AB_907218
CD28 (CD28.2)	BD Biosciences	Cat# 555725; RRID: AB_396068
CD4 (RPA-T4)	BD Biosciences	Cat# 555349; RRID: AB_398593
CD8 (RPA-T8)	BD Biosciences	Cat# 560662; RRID: AB_1727513
CD3 (HIT3a)	BioLegend	Cat# 300330; RRID: AB_10551436
CD45RA (HI100)	BD Biosciences	Cat# 555488; RRID: AB_395879
CD45RO (UCHL1)	BD Biosciences	Cat# 555493; RRID: AB_395884
CCR7 (G043H7)	BioLegend	Cat# 353212; RRID: AB_10916390
IL7Ra (eBioRDR5)	Thermo Fisher Scientific	Cat# 12-1278-41; RRID: AB_10853334
CD62L (DREG-56)	BioLegend	Cat# 304822; RRID: AB_830801
CD25 (M-A251)	BD Biosciences	Cat# 561399; RRID: AB_10643029
CD39 (A1)	BioLegend	Cat# 328218; RRID: AB_2562897
IL-2 (MQ1-17H12)	BD Biosciences	Cat# 560708; RRID: AB_1727543
TNFα (MAb11)	BioLegend	Cat# 502930; RRID: AB_2204079
Granzyme B (GB11)	BD Biosciences	Cat# 560213; RRID: AB_1645453
IFN-γ (4S.B3)	BD Biosciences	Cat# 554552; RRID: AB_395474
BCL6 (K112-91)	BD Biosciences	Cat# 561525; RRID: AB_10898007
TCF1/TCF7 (S33-966)	BD Biosciences	Cat# 564217; RRID: AB_2687845
β-catenin (15B8)	eBioscience	Cat# 50-2567-42; RRID: AB_11218086
p-JNK (T183/Y185; N9-66)	BD Biosciences	Cat# 562480; RRID: AB_11153134
p-S6 (S235/S236; N7-548)	BD Biosciences	Cat# 561457; RRID: AB_10643763
p-AKT (S473; M89-61)	BD Biosciences	Cat# 560343; RRID: AB_1645397
p-mTOR (S2448; O21-404)	BD Biosciences	Cat# 564242; RRID: AB_2738695
p-ERK (T202/Y204; 20A)	BD Biosciences	Cat# 612593; RRID: AB_399876
BLIMP-1 (6D3)	Santa Cruz Biotechnology	Cat# sc-47732; RRID: AB_628168
PDCD4 (600-401-965)	Rockland Immunochemicals	Cat# 600-401-965; RRID: AB_828370
PTEN (138G6)	Cell Signaling Technology	Cat# 9559; RRID: AB_823618
SPRY1 (D9V6P)	Cell Signaling Technology	Cat# 13013
β-actin (13E5)	Cell Signaling Technology	Cat# 4970; RRID: AB_2223172
Bacterial and Virus Strains		
miRZip-scrambled hairpin vector	Systems Biosciences	Cat# MZIP000-PA-1
miRZip-21 anti-miR-21	Systems Biosciences	Cat# MZIP21-PA-1
Biological Samples		
Leukapheresis	Stanford blood center	N/A
Peripheral blood	Healthy volunteers	N/A
Chemicals, Peptides, and Recombinant Proteins		
Lymphoprep	STEMCELL Technologies	Cat# 07851
Fixable Viability Dye	Thermo Fisher Scientific	Cat# 65-0866-14

REAGENT or RESOURCE	SOURCE	IDENTIFIER
Human GM-CSF	R&D Systems	Cat# 215-GM-010
Human IL-4	R&D Systems	Cat# 204-IL-010
Human TNF-α	Peprotech	Cat# 300-01A
Human IL-2	Peprotech	Cat# 200-02
Prostaglandin E2	Sigma	Cat# P0409
SR11302, AP1 inhibitor	Tocris Bioscience	Cat# 2476
MK-2206 2HCl, AKT inhibitor	Selleckchem	Cat# S1078
U0126, ERK inhibitor	Tocris Bioscience	Cat# 1144
Hexadimethrine bromide (polybrene)	Sigma	Cat# H9268
Toxic shock syndrome toxin 1 (TSST-1)	Toxin Technology	Cat# TT606
hsa-miR-21-5p miRCURY LNA miRNA Inhibitor	QIAGEN (Exiqon)	Cat# YI04100689
miRCURY LNA miRNA Inhibitor Control	QIAGEN (Exiqon)	Cat# YI00199006
Critical Commercial Assays		
RosetteSep Human CD4+ T Cell Enrichment Cocktail	STEMCELL Technologies	Cat# 15062
EasySep Human Naive CD8+ T Cell Enrichment Kit	STEMCELL Technologies	Cat# 19158
CD45RO MicroBeads, human	Miltenyi Biotec	Cat# 130-046-001
CD14 MicroBeads, human	Miltenyi Biotec	Cat# 130-050-201
Dynabeads Human T-Activator CD3/CD28	Thermo Fisher Scientific	Cat# 11131D
CellTrace Violet Cell Proliferation Kit	Thermo Fisher Scientific	Cat# C34557
Fixation/Permeabilization Solution Kit	BD Biosciences	Cat# 554714
BD Cytofix Fixation Buffer	BD Biosciences	Cat# 554655
BD Phosflow Perm Buffer III	BD Biosciences	Cat# 558050
Annexin V apoptosis detection kit	BD Biosciences	Cat# 559763
RNeasy Plus Micro Kit	QIAGEN	Cat# 74034
mirVana miRNA Isolation Kit	Thermo Fisher Scientific	Cat# AM1560
Ovation Human FFPE RNA-Seq Library Systems	NuGEN	Cat# 0340, 0341
P3 primary cell Nucleofector Kit	Lonza	Cat# V4XP-3024
Power SYBR Green PCR Master Mix	Thermo Fisher Scientific	Cat# 4367659
Maxima First Strand cDNA Synthesis	Thermo Fisher Scientific	Cat# EP0741
miRCURY LNA RT Kit	QIAGEN (Exiqon)	Cat# 339340
Dual-Luciferase Reporter Assay System	Promega	Cat# E1910
Deposited Data		
RNA-seq data of miR-21^{high} and miR-21^{low} cells	This study	SRA: SRP158689
RNA-seq data of activated naive CD4^{+} T cells from young and older individuals	This study	SRA: SRP158502
Microarray data of VZV-specific CD4^{+} T cells	Qi et al., 2016	GEO: GSE86632
Experimental Models: Cell Lines		
HEK293T	ATCC	Cat# CRL-11268; RRID:CVCL_1926
Oligonucleotides		
SMARTApool c-FOS siRNA	Dharmacon	Cat# M-003265-01-0005

REAGENT or RESOURCE	SOURCE	IDENTIFIER
SMARTApool PDCD4 siRNA	Dharmacon	Cat# M-004438-03-0005
siGENOME Non-Targeting siRNA Pool	Dharmacon	Cat# D-001206-13-05
hsa-miR-21-5p miRCURY LNA miRNA PCR Assay	QIAGEN (Exiqon)	Cat# YP00204230
SNORD48(hsa) miRCURY LNA miRNA PCR Assay	QIAGEN (Exiqon)	Cat# YP00203903
Recombinant DNA		
psPAX2	Addgene	Cat#12260
pMD2.G	Addgene	Cat#12259
AP-1 luciferase reporter plasmid	Addgene	Cat#40342
pRL-SV40 renilla luciferase reporter	Promega	Cat# E2231
Software and Algorithms		
FlowJo	TreeStar	RRID:SCR_008520
Prism	GraphPad Software	RRID:SCR_002798
Website for DREVI software	Krishnaswamy et al., 2014	http://systemsbiology.columbia.edu/center-for-computational-biology-and-bioinformat
Website for gene set enrichment analysis (GSEA) software	The Broad Institute	http://software.broadinstitute.org/gsea/index.jsp